University of Nebraska - Lincoln
DigitalCommons@University of Nebraska - Lincoln

Faculty Publications from the Department of Electrical Engineering

Electrical Engineering, Department of

12-15-1999

Near-band-gap CuPt-order-induced birefringence in $Al_{0.48}Ga_{0.52}InP_2$

Mathias Schubert
University of Nebraska - Lincoln, mschubert4@unl.edu

Tino Hofmann
Semiconductor Physics Group, Faculty of Physics and Geoscience, University of Leipzig, Linne´strasse 5, D-04103 Leipzig, Germany

Bernd Rheinlander
Semiconductor Physics Group, Faculty of Physics and Geoscience, University of Leipzig, Linne´strasse 5, D-04103 Leipzig, Germany

Ines Pietzonka
Department of Inorganic Chemistry, Faculty of Chemistry and Mineralogy, University of Leipzig, Linne´strasse 3-5, D-04103 Leipzig, Germany

Torsten Sass
Department of Inorganic Chemistry, Faculty of Chemistry and Mineralogy, University of Leipzig, Linne´strasse 3-5, D-04103 Leipzig, Germany

See next page for additional authors

Follow this and additional works at: http://digitalcommons.unl.edu/electricalengineeringfacpub

Part of the Electrical and Computer Engineering Commons

Schubert, Mathias; Hofmann, Tino; Rheinlander, Bernd; Pietzonka, Ines ; Sass, Torsten; Gottschalch, Volker; and Woollam, John A., "Near-band-gap CuPt-order-induced birefringence in $Al_{0.48}Ga_{0.52}InP_2$" (1999). *Faculty Publications from the Department of Electrical Engineering.* Paper 28.
http://digitalcommons.unl.edu/electricalengineeringfacpub/28

This Article is brought to you for free and open access by the Electrical Engineering, Department of at DigitalCommons@University of Nebraska - Lincoln. It has been accepted for inclusion in Faculty Publications from the Department of Electrical Engineering by an authorized administrator of DigitalCommons@University of Nebraska - Lincoln.

Authors
Mathias Schubert, Tino Hofmann, Bernd Rheinlander, Ines Pietzonka, Torsten Sass, Volker Gottschalch, and John A. Woollam

This article is available at DigitalCommons@University of Nebraska - Lincoln: http://digitalcommons.unl.edu/electricalengineeringfacpub/28

Near-band-gap CuPt-order-induced birefringence in $Al_{0.48}Ga_{0.52}InP_2$

Mathias Schubert
Center for Microelectronic and Optical Materials Research and Department of Electrical Engineering, University of Nebraska, Lincoln, Nebraska 68588
and Semiconductor Physics Group, Faculty of Physics and Geoscience, University of Leipzig, Linnéstrasse 5, D-04103 Leipzig, Germany

Tino Hofmann and Bernd Rheinländer
Semiconductor Physics Group, Faculty of Physics and Geoscience, University of Leipzig, Linnéstrasse 5, D-04103 Leipzig, Germany

Ines Pietzonka, Torsten Sass, and Volker Gottschalch
Department of Inorganic Chemistry, Faculty of Chemistry and Mineralogy, University of Leipzig, Linnéstrasse 3-5, D-04103 Leipzig, Germany

John A. Woollam
Center for Microelectronic and Optical Materials Research and Department of Electrical Engineering, University of Nebraska, Lincoln, Nebraska 68588
(Received 16 March 1999)

The order-induced birefringence in the near-band-gap spectral range (0.75 to 2.5 eV), and its dependence on the degree of ordering η is reported for $Al_{0.48}Ga_{0.52}InP_2$. Transmission and reflection generalized variable angle spectroscopic ellipsometry, dark-field spectroscopy, and cross-polarized reflectance difference spectroscopy (CRDS) are used to determine precisely the room-temperature dielectric functions for polarization parallel and perpendicular to the ordering direction of a series of spontaneously CuPt-ordered samples grown by metal-organic vapor-phase epitaxy. The CRDS technique is introduced as an approach to sense extremely weak anisotropy at oblique angles of incidence. The observed order birefringence is treated as ''chemical-stress'' induced piezobirefringence. The dielectric function model for piezobirefringence in zinc-blende compounds, and selection rules for the transitions from the $\Gamma_{4,5v}$, $\Gamma_{6(1)v}$, $\Gamma_{6(2)v}$ valence band states to the Γ_{6c} conduction band states, allow excellent modeling of the order birefringence in the near-band-gap spectral region. Thus, explicit treatment of the transition-matrix k dependence, as recently suggested for ordered $GaInP_2$ or $GaInAs_2$, can be avoided. The transition energies, strengths, and broadening parameters for the three zone-center transitions are obtained from analysis of the sample dielectric function tensor. All parameters in the quasicubic perturbation model can be fitted. We find, in excellent agreement with recent theoretical predictions, that the spin-orbit splitting parameter of 76 meV is nearly ordering independent, and that the ratio of the crystal-field splitting to the band-gap reduction for the perfectly ordered alloy amounts to 0.62. The band gap of the disordered compound is extrapolated to 2.195 eV. [S0163-1829(99)04647-0]

I. INTRODUCTION

Long-range chemical ordering is widely observed in ternary or quaternary III-V semiconductor compounds grown by metal-organic vapor-phase epitaxy.[1] The spontaneous arrangement of column-III elements in alternating $\{111\}_B$ planes constitutes ordering of the $CuPt_{(B)}$ type in $(A_yB_{1-y})^{III}C^{III}D_2^V$ zinc-blende compounds such as $Al_yGa_{1-y}InP_2$, or $Al_yGa_{1-y}InAs_2$. The stacking direction of the superlattice planes is usually found according to ordering within either one of the $\{111\}_B$ planes, i.e., parallel to the $[\bar{1}11]$ or the $[1\bar{1}1]$ direction (Fig. 1, hereafter referred to as CuPt type). The ordered phase consists of a 1,1 superlattice of monolayer planes $(A_yB_{1-y})_{x+\eta/2}C_{x-\eta/2}$ and $(A_yB_{1-y})_{x-\eta/2}C_{x+\eta/2}$, where x and y are the composition parameters of the random $(A_yB_{1-y})_xC_{1-x}D$ alloy, and η is the difference between the compositions x of two subsequent sublattice planes within the CuPt superlattice. A perfect alternate stacking of the superlattice planes has not yet been reported. Only partially ordered epilayers are formed during the growth process. For partially ordered material the parameter η can be used to quantify the degree of ordering.[2] Two other possible, but rarely observed variants are due to ordering within the $\{111\}_A$ planes ($CuPt_A$). Numerous theoretical and experimental effort has been undertaken in the past to predict and study the effect of chemical ordering on the physical properties of the compound materials.[1,3–7] The most commonly observed consequences of CuPt ordering are the reduction of the fundamental band gap, and the splitting of the valence bands.[4,8–12] Most recently, Wei and Zunger predicted the spontaneous CuPt ordering-induced band-gap reduction ΔE_g relative to the random alloy, crystal-field splitting Δ_{cf} at the valence band maximum, and change of spin-orbit splitting Δ_{so} for $AlInP_2$, $AlInAs_2$, $GaInP_2$, and $GaInAs_2$ using the corrected local density approximation.[7]

Similar to (111)-biaxial strain, CuPt ordering splits and

 ©1999 The American Physical Society

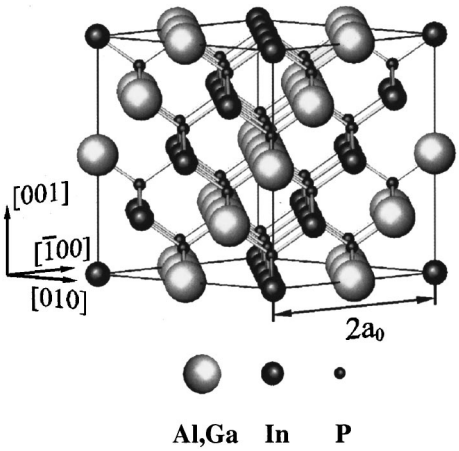

FIG. 1. Crystal structure of perfectly $CuPt_{(B)}$ ordered $Al_yGa_{1-y}InP_2$ for ordering along the $[1\bar{1}\bar{1}]$ direction.

shifts the zinc-blende states, e.g., near the valence-band maximum, and leads to polarized interband transitions.[3,4] Although the interpretation of the order-induced valence-band states $|\Gamma_{4,5v}\rangle$, $|\Gamma_{6(1)v}\rangle$, and $|\Gamma_{6(2)v}\rangle$ is different from the case of biaxial strain along $\langle 111\rangle$, the Hamiltonian used to calculate the energy level shift and transition matrix elements has the same form as that for stress applied along, e.g., [111]. It has been shown previously that fictitious internal strain and deformation potentials can be treated as functions of the order parameter η.[2,4] In general, nondegenerate polarized interband transitions will induce optical birefringence, especially below the fundamental band-to-band transitions. Furthermore, polarization selection rules for optical transitions cause dichroic material properties, since the strength of photonic absorption will depend on the direction of polarization.[13] The dielectric function of materials with lowered symmetry is then represented by a complex rank-2 tensor. This is well known for, e.g., the stress-induced birefringence (piezobirefringence) in cubic semiconductors. For analysis of the piezobirefringence in zinc-blende semiconductors, Higginbotham, Cardona, and Pollak developed an interband one-electron model for the dielectric function, including the effects of dispersion of the E_0-, E_1-, and E_2-type transitions.[14] This model contains critical-point transition energies, their strength, and broadening values as adjustable parameters. Quantitative analysis of anisotropy measurements then allows for determination of level splitting and transition strength as a function of strain.

Direct measurement of CuPt-order-induced birefringence has been reported by Wirth *et al.* for spontaneously ordered $GaInP_2$ and $Al_{0.33}Ga_{0.67}InP_2$.[15] The authors investigated waveguide structures and observed a positive birefringence with small magnitude far below the band gap of the alloys. Also, a sign change of the birefringence was found when approaching the band gap. A six-band *kp* method using the Hamiltonian proposed by Wei and Zunger[16] was used for qualitative description of the birefringence below the band gap. However, the waveguide experiment failed to explore the zone-center transition energies because of absorption at the fundamental gap transition.

Several authors observed characteristic anisotropy features in polarized reflection and transmission spectra for photon energies near and across the fundamental direct-gap transitions. Luo *et al.* used reflectance-difference spectroscopy (RDS) for assignment of band-gap reduction and valence-band splitting values in ordered $GaInP_2$ samples. The RD spectra were compared with four-band, six-band, and eight-band *kp* calculations, which also included explicit *k* dependence of the interband transition matrix elements.[17,18] However, none of these models provided good fits to the experimental data. In particular, the $|\Gamma_{6(1)v}\rangle$ and $|\Gamma_{6(2)v}\rangle$ state transition features remained unexplained for the RD spectra. Schubert *et al.* reported recently on the application of cross-polarized transmission spectra of spontaneously ordered $GaInP_2$ and $AlInP_2$ for the determination of the band-gap reduction and valence-band splitting in samples with different degrees of ordering.[11,19] But quantitative analysis of the order-induced anisotropy was not performed. So far, the spectral dependence of the dielectric functions in the near-band-gap spectral range is unknown for CuPt-ordered III-V compounds. Other techniques, which avoid explicit treatment of the sample dielectric function tensor, have been employed to determine the order-affected zone-center transition energies. Wirth *et al.* used measurement of linear absorption anisotropy for determination of band-gap reduction and valence-band splitting in ordered $GaInAs_2$ grown on InP substrates.[20,21] The optical fingerprints of CuPt-ordered $GaInP_2$ have been measured by many authors.[3] Recently, Mascarenhas *et al.*[22] and Kiesel *et al.*[23] obtained the transition energies from all valence band states as a function of ordering η using low-temperature nonlinear exciton absorption bleaching and polarization-dependent electroabsorption measurements, respectively. The dependencies of gap-reduction and level-splitting values on η were found to be in excellent agreement with the theoretical predictions by Wei and Zunger.[7] Except for $GaInP_2$ and $AlInP_2$, none of the optical CuPt fingerprints, i.e., the amount of the gap reduction and the increase of spin splitting and crystal-field splitting vs η, have been observed for any composition of the $Al_yGa_{1-y}InP_2$ alloy system. The present work focuses on the exploitation of the optical CuPt fingerprints in $Al_{0.48}Ga_{0.52}InP_2$. The generalized ellipsometry approach is used to measure sample anisotropy. Additionally, approximate equations for the light propagation in CuPt order-birefringent films are presented which allow analysis of polarized reflection and transmission spectra. As a result, we are able to complete quantitative analysis of the order-induced birefringence in the near-band-gap spectral range. For analysis of the anisotropic dielectric function of the chemically ordered compounds, we apply the piezobirefringence model. The dielectric functions for polarization parallel and perpendicular to the ordering direction are reported as a function of ordering η. Finally, we obtain the optical transition energies from all three valence band states as a function of ordering η. The parameters in the quasicubic perturbation model are reported for $Al_{0.48}Ga_{0.52}InP_2$, and compared to those predicted by Wei and Zunger.

II. THEORY

A. Model dielectric function of CuPt-ordered alloys (order-birefringence)

The largest optical structure to be discussed in this paper arises from the transitions at the center of the Brillouin zone

(E_0-type transitions, $E_0^{(1)}:\Gamma_{4,5v}-\Gamma_{6c}$, $E_0^{(2)}:\Gamma_{6(1)v}-\Gamma_{6c}$, $E_0^{(3)}:\Gamma_{6(2)v}-\Gamma_{6c}$). The transitions along the $\langle 111\rangle$ directions in **k** space (E_1-type),[24] have also been demonstrated, both theoretically and experimentally, to split into at least three transitions upon ordering.[5,25] These transitions are located outside the spectral range investigated here. However, their contributions to the dielectric functions below the fundamental transitions may become appreciable. The strong E_1-type transitions likely cause long-tail birefringence that extends far below the fundamental band gap when polarized by symmetry reduction such as CuPt ordering. The feature in zinc-blende compounds labeled with E_2 contains contributions from transitions within a large region of the Brillouin zone superimposed by weak transitions between the valence bands and larger conduction bands close to the center, and along the $\langle 111\rangle$ directions.[24] Recent theoretical calculations predict ordering-induced splitting and shifting of these transitions as well.[5] We therefore will consider all of the E_0-, E_1-, and E_2-type contributions to the dielectric function of the CuPt-orderd compound; since in general these transitions may cause anisotropy, although we observe appreciable information from the E_0-type transitions only.

In the one-electron model, the imaginary part of the dielectric function $\in_2(\omega)$ in the vicinity of a critical point n is related to the joint-density-of-states $\rho_{c,v}(\hbar\omega)$, and the momentum (dipole transition) matrix elements $\langle c|p_j|v_i\rangle$ between states at the maximum of the valence bands $|v_i\rangle$ and the conduction band minimum $|c\rangle$:

$$\in_2(\omega)_j \propto \sum_i |\langle c|p_j|v_i\rangle|^2 \rho_{c,v}(E). \tag{1}$$

The index j refers to the component of momentum polarized parallel to either axis of a right-handed cartesian coordinate system. Parabolic bands and matrix elements are assumed to be independent of k. The contribution of the transition i at a critical point n to the major complex dielectric function $\in(\omega)_j$ may be written as[24]

$$[\in(\omega)]_j \propto \in_{\infty,j} + \sum_{i,n} A_{jn}^{(i)} f_n^{(i)}(\chi_n^{(i)}), \tag{2}$$

with $\chi_n^{(i)}=(E+i\Gamma_n^{(i)})/E_n^{(i)}$. The $f_n^{(i)}$ are well-known functions for the E_0-, E_1-, and E_2-type transitions in zinc-blende semiconductors.[14,27] The quantities $A_{jn}^{(i)}$, $\Gamma_n^{(i)}$, and $E_n^{(i)}$ are treated as, respectively, strength, broadening, and energy of transition i at critical point n due to incident electromagnetic radiation polarized along $j=x,y,z$. The ''static'' dielectric constants $\in_{\infty j}$ correspond to hf electric fields applied parallel to j. Due to the type of symmetry of CuPt-ordered compounds, the order birefringence is uniaxial. Therefore, critical-point parameters, and dielectric constants are identical for polarization parallel (1-11). In this work we consider single-variant CuPt ordering only.[26] Subsequent symbols which correspond to polarization parallel (perpendicular) to the ordering direction will be labeled by ''∥'' (''⊥'').

(i) E_0 transitions ($n=0$): The contributions of the zone-center transitions to the complex dielectric functions in Eq. (2) are obtained with[14]

$$f_0^{(i)}(\chi_0^{(i)})=[E_0^{(i)}]^{-1.5}(\chi_0^{(i)})^{-2}[2-\sqrt{1+\chi_0^{(i)}}-\sqrt{1-\chi_0^{(i)}}]. \tag{3}$$

In the case of CuPt ordering, the splitted states at the valence-band maximum are the twofold (spin) degenerate $\Gamma_{4,5v}$, $\Gamma_{6(1)v}$, and $\Gamma_{6(2)v}$ states (figuratively ''heavy-hole'' like, ''light-hole'' like, and ''spin-split'' like), respectively. Direct absorption at the M_0 critical points is due to transitions from the maximum of the valence bands to the twofold-degenerate s-like conduction band minimum at $\mathbf{k}=0(\Gamma_{6c})$. The $\Gamma_{6(1)v}$ and $\Gamma_{6(2)v}$ states lie at energies $\delta E_{12}=E_0^{(1)}-E_0^{(2)}$ and $\delta E_{13}=E_0^{(1)}-E_0^{(3)}$ below the lowest absorption edge $E_0^{(1)}$. The transition $E_0^{(1)}=\Gamma_{4,5v}-\Gamma_{6c}$ is forbidden for polarization parallel to the ordering direction only. The transitions $E_0^{(2)}=\Gamma_{6(1)v}-\Gamma_{6c}$, and $E_0^{(3)}=\Gamma_{6(2)v}-\Gamma_{6c}$ may be polarized parallel as well as perpendicular to the ordering direction.[10] Hence, for each polarization j (major dielectric function $\in_j$) the summation in Eq. (2) includes contributions from three transitions. Excitonic effects are known to modify the absorption edges of semiconductors even at room temperature. We do not include, however, contributions of exciton absorption to the imaginary part of the E_0-type transitions since none of the samples revealed appreciable excitonic absorption features. We suppose from our experiments that excitons in $Al_{0.48}Ga_{0.52}InP_2$ become thermally ionized at room temperature, and therefore do not contribute to the order birefringence.

(ii) E_1 transitions ($n=1$): The contributions of the transitions along the $\langle 111\rangle$ directions to the complex dielectric functions are usually modeled by two-dimensional M_0 critical-point approximations, which enter Eq. (2) as follows:[14]

$$f_1^{(i)}(\chi_1^{(i)})=-(\chi_1^{(i)})^{-2}\ln[1-(\chi_1^{(i)})^2]. \tag{4}$$

Wei, Franceschetti, and Zunger[5] predict that for CuPt ordering, the E_1 transitions split into $E_1^{(1)}$ and $E_1^{(2)}$ components along the zinc-blende Λ lines which connect Γ with $L^*\{\pi/a(\text{-}111),\pi/a(1\text{-}11),\pi/a(11\text{-}1)$, a being the lattice constant}, and an $E_1^{(3)}$ component along the ordering direction. Transitions with small density of states ($E_1^{(4)}$) may also occur along the Λ line between $\Gamma-L_{111/2}$, and $L_{111}-L_{111/2}$.[5] The $E_1^{(1)}$ and $E_1^{(2)}$ transitions are predicted to have nonzero strength parameter for polarization perpendicular to the ordering direction only, whereas the $E_1^{(3)}$ and $E_1^{(4)}$ transitions are allowed for all polarization directions. To obtain the complex dielectric function for each polarization, the right side of Eq. (2) may consist of four terms for $n=1$. Transitions which are attributed to M_1 critical points are strongly modified by excitonic effects. Adachi suggested the usage of Lorentzian line shapes to model contributions of Wannier-type two-dimensional (2D) ground-state excitons. Those may find consideration at each E_1-type transition.[24,27,28]

(iii) E_2 transitions ($n=2$): Although outside the spectral range of interest here, these transitions possess large amplitudes since they comprise contributions within a large range of the Brillouin zone. The dispersion from E_2-type transitions in zinc-blende semiconductors is usually treated as that of a single damped harmonic oscillator (DHO). To account for order-induced splitting and shifting of states in the disordered alloy, the contributions to $\in$ may be summed over

TABLE I. Sample structure parameters for the $Al_{0.48}Ga_{0.52}InP_2$ epilayers. The samples were deposited at $T_G = 720\,°C$, and different substrate miscuts were included. The epilayers are nearly lattice matched to GaAs [perpendicular mismatch $(\Delta a/a)_\perp$ in column 5]. The thickness d of the as-grown (A) and on-glass (G) epilayers are obtained from ellipsometry data analysis. The order parameter η is obtained from scaling the lowest zone-center transition energy ($E_0^{(1)}$ in Table II) to a maximum band-gap reduction of 353 meV, which is the linear average for $Al_yGa_{1-y}InP_2$ for $y=0.48$ between the values for $GaInP_2$ (430 meV), and $AlInP_2$ (270 meV) predicted by Wei and Zunger (Ref. 7). The random alloy bandgap is obtained as 2.195 eV (see also Table III).

Sample	Substrate miscut	Surface normal	Θ	$(\Delta a/a)_\perp$ (10^{-4})	η	$d(A)$ [nm]	$d(G)$ [nm]
1	0°→(100)	[0 0 1]	54.7°	8.6	0.53	1170±1	1121±1
2	2°→(101)	[1 0 29]	53.3°	6.4	0.51	1162±2	1150±2
3	6°→(101)	[2 0 19]	50.6°	4.1	0.47	1210±1	1144±1
4	6°→(111)	[2 2 27]	55.0°	3.7	0.39	1225±2	1200±1

DHO terms which may account for transitions polarized parallel or perpendicular to the ordering direction:

$$f_2^{(i)}(\chi_2^{(i)}) = (1-[\chi_2^{(i)}]^2)^{-2}, \quad \Gamma_2^{(i)} \ll E_2^{(i)}. \tag{5}$$

B. Optical fingerprints of CuPt-ordered alloys

Optical properties can be used to estimate the relative degree of ordering within alloys of the same composition.[1,3,4] We briefly recall here what has been termed *optical fingerprints* of ordered alloys, and which have been introduced and derived for, e.g., the III-As and III-P by Wei, Zunger, and coworkers (See, e.g., Refs. 1, 4, 5, 6, and 7). The most eminent feature of ordering is the reduction of the fundamental band gap $\Delta E_g = E_g^{(\eta)} - E_g^{(\eta=0)}$, which has been shown to scale with the degree of ordering η,

$$\Delta E_g^{(\eta)} = \Delta E_g^{(\eta=1)} \eta^2, \tag{6}$$

where $\Delta E_g^{(\eta=1)}$ is the maximum gap reduction relative to the random alloy.[6] The valence-band splitting δE_{ij} at the top of the valence band for CuPt ordering has been described by Wei and Zunger using the quasicubic perturbation model:[4]

$$\delta E_{12} = \frac{1}{2}(\Delta_{CF}+\Delta_{SO}) - \frac{1}{2}\sqrt{(\Delta_{CF}+\Delta_{SO})^2 - \frac{8}{3}\Delta_{CF}\Delta_{SO}}, \tag{7}$$

$$\delta E_{13} = \frac{1}{2}(\Delta_{CF}+\Delta_{SO}) + \frac{1}{2}\sqrt{(\Delta_{CF}+\Delta_{SO})^2 - \frac{8}{3}\Delta_{CF}\Delta_{SO}}, \tag{8}$$

$$\Delta E_{23} = \sqrt{(\Delta_{CF}+\Delta_{SO})^2 - \frac{8}{3}\Delta_{CF}\Delta_{SO}}, \tag{9}$$

where Δ_{SO} and Δ_{CF} are treated as the spin-orbit, and crystal-field splitting parameters, respectively. These quantities are assumed to scale with η:

$$\Delta_{SO}^{(\eta)} = \Delta_{SO}^{(\eta=0)} + \delta\Delta_{SO}^{(\eta=1)}\eta^2, \tag{10}$$

$$\Delta_{CF}^{(\eta)} = \delta\Delta_{CF}^{(\eta=1)}\eta^2, \tag{11}$$

and therefore allow for their determination using the experimentally determined quantities δE_{ij}. However, if the degree of ordering of a given sample is unknown, only the ratios

$$\xi^{-1} = -\delta\Delta_{SO}^{(\eta=1)}/\Delta E_g^{(\eta=1)}, \quad \zeta^{-1} = -\delta\Delta_{CF}^{(\eta=1)}/\Delta E_g^{(\eta=1)}. \tag{12}$$

can be obtained.[7]

III. EXPERIMENTAL DETAILS AND TECHNIQUES

A. Sample preparation

The growth of the $Al_{0.48}Ga_{0.52}InP_2$ samples was performed on (001)-GaAs with different miscuts by low-pressure metal-organic vapor-phase epitaxy (MOVPE) at 720 °C in a horizontal reactor with a rotating substrate holder. The substrate orientations and sample parameters, such as the inclination of the ordering direction from the sample normal, are given in Table I. The input gas-flow ratio $f(V)/f(III)$ was 334. Trimethylaluminium, triethylgallium, and trimethylindium were used as group-*III* sources, and phosphine as group-*V* precursor. Prior to the epilayer growth a GaAs-buffer layer of about 300-nm thickness was deposited. The relative composition of Al and Ga was controlled by adjusting the gas flows of trimethylaluminium ($x_{V(Al)} = 0.244$), and triethylgallium ($x_{V(Ga)} = 0.266$).

The perpendicular lattice mismatch $[\Delta a/a]_\perp$ of the epilayer to the GaAs substrate was measured by double-crystal x-ray diffraction using the (004)-reflex of both the substrate and the epilayer. The film thickness estimated from the growth rate was 1.2 μm. The CuPt ordering in the samples was observed in selected area diffraction pattern and dark-field transmission electron microscopy images. The selected area [110]-pole diffraction pattern showed additional spots due to the alternating sublattice planes in almost only the $[1\bar{1}1]$ direction (single-variant ordering in samples 2, 3, 4,), and the $[\bar{1}11]$ direction (double-variant ordering in sample 1).[26,29] Dark-field transmission electron microscopy images revealed that the ordered atomic arrangement is distributed across almost the entire epilayer.

One piece of each sample was placed upside down on a thin glass slide, and the substrate material was etched from the back side as explained in Refs. 11 and 19. Although the etch process was stopped immediately after approaching the

epilayer, the latter was unintentionally thinned as well. The thicknesses of the $Al_{0.48}Ga_{0.52}InP_2/GaAs$ (samples labeled with *A*) and the $Al_{0.48}Ga_{0.52}InP_2$/glass (samples labeled with *G*) epilayers were determined during data analysis, and are given in Table I.

B. Generalized ellipsometry

Standard ellipsometry at oblique angle of incidence Φ_a determines the ratio ρ of the complex *p*-and *s*-polarized reflectance coefficients $\mathbf{r}_p$ and $\mathbf{r}_s$ from layered systems with plane parallel interfaces:[30]

$$\rho=\frac{r_p}{r_s}=\tan\Psi\exp\{i\Delta\}. \tag{13}$$

Nondepolarizing samples which contain anisotropic materials can be treated within the Jones matrix approach. Here, a 2×2 complex matrix, the so-called Jones matrix, relates any incident state of polarization with the corresponding state of polarization transmitted or reflected upon the sample. Standard ellipsometry, however, fails to explore the Jones matrix properties of anisotropic samples. A more comprehensive approach, which has been termed generalized ellipsometry, allows simultaneous determination of the normalized Jones matrix elements. This technique combines the advantages of ellipsometry to monitor accurately thin-film optical properties with the ability to obtain dielectric function tensor components, and its spatial coordinates in arbitrarily anisotropic layered samples.[31] For anisotropic surfaces, the complex reflectance ratio ρ depends on the incident polarization state χ, and the normalized Jones matrix elements[30]

$$\rho=(\mathbf{R}_{pp}+\mathbf{R}_{sp}\chi^{-1})/(1+\mathbf{R}_{pp}\mathbf{R}_{ps}\chi). \tag{14}$$

Generalized (reflection) ellipsometry determines the normalized but complex-valued ratios $\mathbf{R}_{pp}$, $\mathbf{R}_{ps}$, and $\mathbf{R}_{sp}$, which are defined as follows:[32]

$$\frac{\mathbf{r}_{pp}}{\mathbf{r}_{ss}}\equiv\mathbf{R}_{pp}=\tan\Psi_{pp}\exp\{i\Delta_{pp}\},$$

$$\frac{\mathbf{r}_{ps}}{\mathbf{r}_{pp}}\equiv\mathbf{R}_{ps}=\tan\Psi_{ps}\exp\{i\Delta_{ps}\},$$

$$\frac{\mathbf{r}_{sp}}{\mathbf{r}_{ss}}\equiv\mathbf{R}_{sp}=\tan\Psi_{sp}\exp\{i\Delta_{sp}\}, \tag{15}$$

and which, at a given photon energy *E*, angle of incidence Φ_a, and sample azimuth φ form an irreducible set for sample anisotropy information. (The generalized transmission ellipsometry ratios are obtained by substituting the Jones reflection coefficients with their respective transmission ratios.) For a detailed introduction into the generalized ellipsometry technique, the reader is referred to previous work in which the definition of all quantities, the coordinate system, and the mathematical framework used for analysis of birefringent thin films have been presented and discussed in detail.[31,32,33,34,35] Briefly, the plane of incidence, the sample surface, and the sample normal span a right-handed coordinate system, where *z* points toward the substrate, and *x* is in the plane of incidence. In this study, the sample azimuth φ in this notation is the angle between the *x* axis and the projection line of the $[1\bar{1}1]$ onto the sample surface. The inclination of the $[1\bar{1}1]$ with respect to the sample normal is described by the Euler angle Θ.

The ellipsometric spectra were measured at multiple angles of incidence ($\Phi_a=0°$ in transmission; $\Phi_a=15°$, and 65° in reflection arrangement) by generalized variable angle spectroscopic ellipsometry (GVASE), and the samples were constantly aligned to the laboratory coordinate system with $[100]\|x$, $[0\bar{1}0]\|y$, and $[00\bar{1}]\|z$. The same sample setup is used for CRDS and DFS data acquisition, and we will refer to this setup as CRDS setup. Note that *y* and *z* invert accordingly for the samples on glass. (See Fig. 1).

A recently reported 4×4 matrix formalism is employed for data analysis.[33] It is shown within the appendix that, to first order approximation in $\Delta\in$, the GVASE data types $\mathbf{R}_{ps}$ and $\mathbf{R}_{sp}$ are proportional to the order-birefringence $\Delta\in=\frac{1}{3}\in_{\|}-\frac{1}{3}\in_{\perp}$, whereas $\mathbf{R}_{pp}$ evolves linearly in $\Delta\in$ from the isotropic ellipsometric ratio $\rho^{is}=\mathbf{r}_p/\mathbf{r}_s$:

$$R_{ps}=\Delta\in(\beta_r+i\beta_i)_{ps}+O[(\Delta\in)^2], \tag{16a}$$

$$R_{sp}=\Delta\in(\beta_r+i\beta_i)_{sp}+O[(\Delta\in)^2], \tag{16b}$$

$$R_{pp}=\rho^{is}[1+\Delta\in(\beta_r+i\beta_i)_{pp}+O((\Delta\in)^2)]. \tag{16c}$$

The coefficients β_r and β_i, as well as the isotropic reflection coefficients $\mathbf{r}_p$ and $\mathbf{r}_s$, depend on the angle of incidence Φ_0, the mean value of the major dielectric functions $\in=\frac{2}{3}\in_{\perp}+\frac{1}{3}\in_{\|}$, the film thickness *d*, and the dielectric function of the substrate $\in_s$. The coefficients β_r and β_i possess some similarity with those known as Seraphin coefficients for isotropic semiconductor surfaces.[36] The coefficients β_r and β_i for CuPt-type order-birefringent thin films grown on isotropic substrates are given in the appendix of the present work.

C. Dark-field spectroscopy

A cross-polarized transmission technique has been introduced recently to study the order birefringence of spontaneously ordered $GaInP_2$ and $AlInP_2$ alloys.[11,19] We named this approach ''dark-field'' spectroscopy (DFS) because of the extremely weak intensities transmitted upon the spectrally local dichroic and linear birefringence centered at the fundamental direct-gap transitions of the ordered alloys. The spectral features observed have been pointed out as inherent to the ordered state within the CuPt-ordered III-V compounds. For this experiment, the sample is released from the substrate and placed upside down on a glass slide. In the present work we use this technique to study $Al_{0.48}Ga_{0.52}InP_2$. The sample alignment is the same as for the GVASE and CRDS acquisition procedure (i.e., the CRDS setup), and experimental details have been discussed elsewhere.[11] We demonstrate within the appendix of the present work that, to first order approximation in $\Delta\in$, the DFS data of a CuPt-ordered film are proportional to $\|\Delta\in\|=\Delta\in\Delta\in^*$:

$$\mathrm{DFS}\sim\|\Delta\in\|\|\alpha_r+i\alpha_i\|+O(\|\Delta\in\|^2). \tag{17}$$

The coefficients α_r and α_i depend on $\in$, *d*, and $\in_s$. Knowledge of the spectral dependence of the averaged CuPt-

ordered material dielectric function $\in$, and the film thickness d is necessary to unambiguously analyze data.

D. Cross-polarized reflectance-difference spectroscopy

In this paper, a cross-polarized reflectance difference spectroscopy (CRDS) technique is introduced which allows for detection of extremely small in-plane birefringence of thin films. The motivation for development of the CRDS technique is to avoid the wet-chemical substrate removal. However, because of the nearly index-matched GaAs substrate, the cross-polarized reflection coefficients, which contain similar information about the order-birefringence as the DFS data, are smaller in magnitude and harder to retrieve. We therefore employ a modulation approach.[37] A detailed description of this technique will be given elsewhere. Briefly, the sample surface is irradiated at oblique incidence by a collimated and linearly polarized (polarizer P) light beam. The reflected light beam passes a second linear polarizer (analyzer A), and its remaining intensity is detected as a function of photon energy. Polarizer and analyzer vary slightly by $|\gamma_p|$, $|\gamma_a| \ll \pi$ from the p-s cross-polarized setup (P, A are p or s polarized if their azimuth orientation, with respect to the plane of incidence, is 0 or $\pi/2$, respectively.). The detected intensity is approximated as follows [according to, e.g., Eq. (10) in Ref. 32]:

$$I(\gamma_p,\gamma_a)_{ps} \equiv I(P=\gamma_p, A=\pi/2+\gamma_a) \sim |-\gamma_a(r_{pp}+\gamma_p r_{sp}) + (r_{ps}+\gamma_p r_{ss})|^2, \tag{18}$$

where $\mathbf{r}_{ij}$ $(i,j=\text{‘‘}p,\text{’’’’}s\text{’’})$ are the complex reflection coefficients.[30] For small off-diagonal reflection coefficients $(\|\mathbf{r}_{ps}\|,\|\mathbf{r}_{sp}\| \ll \|\mathbf{r}_{pp}\|,\|\mathbf{r}_{ss}\|)$, and neglecting second order terms in $\gamma_p=\gamma_a=\gamma$, the symmetric set of four intensity measurements $I(\pm\gamma,\pm\gamma)_{ps}$, and $I(0,0)_{pp}$ yield $\mathrm{Re}(\mathbf{R}_{ps})$

$$\mathrm{Re}\left\{\frac{r_{ps}}{r_{pp}}\right\} \equiv \frac{\Delta R}{R} = \frac{I(-\gamma,-\gamma)_{ps}+I(-\gamma,\gamma)_{ps}-I(\gamma,\gamma)_{ps}-I(\gamma,-\gamma)_{ps}}{8\gamma I(\gamma=0,\ \gamma=0)_{pp}}, \tag{19}$$

where $\mathrm{Re}\{a\}$ denotes the real part of a complex a. Likewise, if P and A are, respectively, nearly s and p polarized, $\mathrm{Re}\{\mathbf{R}_{sp}\}$ is obtained through a similar set:

$$\mathrm{Re}\left\{\frac{r_{sp}}{r_{ss}}\right\} \equiv \frac{\Delta R}{R} = \frac{I(\gamma,\gamma)_{sp}+I(\gamma,-\gamma)_{sp}-I(-\gamma,-\gamma)_{sp}-I(-\gamma,\gamma)_{sp}}{8\gamma I(\gamma=0,\ \gamma=0)_{ss}}. \tag{20}$$

We define the right sides of Eqs. (19) and (20) as the two CRDS data types used in this work. This approach provides spectral information on extremely small reflectance anisotropy at oblique angles of incidence. But, accurate polarizer and analyzer adjustment is a prerequisite. The effect of this difference technique is to quench the strong on-diagonal reflectivity $\mathbf{r}_{pp}$ and $\mathbf{r}_{ss}$. The sample itself then becomes a polarization modulator. If the sample reflectivity is purely isotropic, the numerators in Eqs. (19) and (20) are antisymmetric and cancel out, even at oblique incidence. The latter distinguishes this approach from the well-established reflectance difference spectroscopy (RDS) technique which relies on the normal incidence setup. RDS detects the set of p to p and s to s reflectivity ($\mathbf{r}_{pp}$ and $\mathbf{r}_{ss}$), and the weighted difference $(\mathbf{r}_{pp}-\mathbf{r}_{ss})/(\mathbf{r}_{pp}+\mathbf{r}_{ss})$ is supposed to vanish for isotropic surfaces.[37,38,39] If a CuPt-ordered thin film is oriented to the plane of incidence according to $[100]\|x$, $[0\bar{1}0]\|y$, and $[00\bar{1}]\|z$, the CRDS signal is to first-order approximation linear in $\Delta\in$:

$$\left[\frac{\Delta R}{R}\right]_{ps;sp} = \mathrm{Re}[\Delta\in(\beta_r+i\beta_i)]_{ps;sp}+O[(\Delta\in)^2], \tag{21}$$

and the coefficients β_r and β_i are the same as in Eqs. (16a) and (16b).

E. Reflectance-difference spectroscopy

In cubic semiconductors, RDS can be used to detect surface-induced anisotropy, whereas in noncubic materials, the reflectance difference is usually dominated by bulk anisotropy.[40] RDS data from CuPt-ordered samples are commonly obtained by acquiring reflectance for polarization parallel $[1\bar{1}0](R_{[1\bar{1}0]})$ and $[110](R_{[110]})$:

$$\Delta R/R = 2\frac{R_{[1\bar{1}0]}-R_{[110]}}{R_{[1\bar{1}0]}+R_{[110]}}. \tag{22}$$

In the Jones matrix element notation this signal refers to $\Delta R/R = 2(\|\mathbf{r}_{pp}\|-\|\mathbf{r}_{ss}\|)/(\|\mathbf{r}_{pp}\|+\|\mathbf{r}_{ss}\|)$; $\|\mathbf{r}\|=\mathbf{r}\mathbf{r}^*$. According to the frame of reference used here, the ordering direction is within the (x-z) plane (hereafter referred to as RDS setup). For small order-birefringence $\Delta\in$, the RD spectrum of a thin-film sample is composed of an isotropic term, which vanishes at normal incidence only, and a second term which is linear in $\Delta\in$ (see Appendix):

$$\frac{\Delta R}{R} = \left[\frac{\Delta R}{R}\right]_{is} + \mathrm{Re}\{\Delta\in(\beta_r+i\beta_i)\}+O[(\Delta\in)^2]. \tag{23}$$

Both terms depend on the angle of incidence Φ_a, the averaged CuPt-ordered material dielectric function $\in$, the film thickness d, and $\in_s$. Consideration of interference effects, and knowledge of the isotropic contribution due to $\in$ are necessary for analysis of experimental RD spectra. The coefficients β_r and β_i in Eq. (23) are different from those in Eq. (21) because of the different sample orientation during the CRDS and RDS measurements. Those for Eq. (23) are given in the appendix as well.

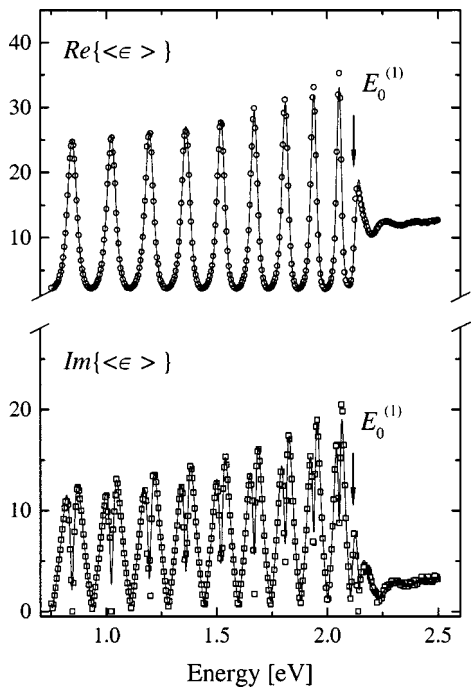

FIG. 2. Pseudodielectric function $\langle \in \rangle$ of a CuPt-ordered $Al_{0.48}Ga_{0.52}InP_2$ epilayer on glass (sample $G3$) obtained from a single-angle-of-incident standard ellipsometry measurement at fixed incident polarization ($\Phi_a = 65°$; $\chi = 1$; ○ $\mathrm{Re}\langle \in \rangle$, □ $\mathrm{Im}\langle \in \rangle$, —— best fit). The standard ellipsometry data reveal the lowest direct transition $\Gamma_{4,5v} - \Gamma_{6c}$ at $E_0^{(1)}$ only, where the interference oscillations begin to disappear. The data also provide the mean value of the major $Al_{0.48}Ga_{0.52}InP_2$ dielectric functions, and thickness of the epilayer, which are prerequisites for analysis of the generalized ellipsometry data.

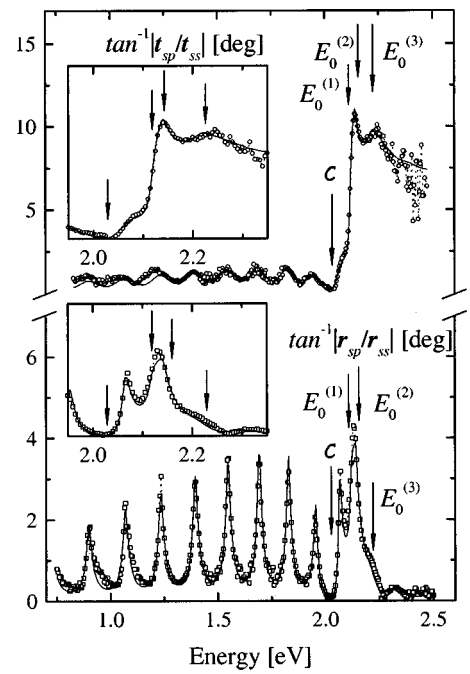

FIG. 3. Transmission (○; $\Phi_a = 0°$) and reflection (□; $\Phi_a = 15°$) GVASE data Ψ_{sp} from sample $G3$ (—— best fit). The insets enlarge the zone-center transition region. The data sets are fingerprints of the near-band-gap CuPt-order-induced birefringence. Below the first zone-center transition energy $E_0^{(1)}$, the birefringence is real valued and undergoes a sign change indicated by C. Below C, the birefringence is positive. Above C, the order birefringence has strong dispersion, and becomes complex valued at $E_0^{(1)}$. Absorption of incident electric field polarizations along the sublattice planes entails the strong rise in $\mathbf{t}_{sp}$ (upper panel in Fig. 5) and $\tan^{-1}|\mathbf{t}_{sp}/\mathbf{t}_{ss}|$. At $E_0^{(2)}$, the incident radiation polarized along the ordering direction excites electrons from the $\Gamma_{6(1)v}$ valence-band state to the Γ_{6c} conduction band state, bleaching the *p-s* mode coupling effects above $E_0^{(2)}$. The $\Gamma_{6(2)v} - \Gamma_{6c}$ transition is activated at $E_0^{(3)}$. Above $E_0^{(3)}$, the film becomes opaque.

IV. RESULTS

A. Standard ellipsometry

Figure 2 presents standard ellipsometry data acquired at $\Phi_a = 65°$ from a CuPt-ordered $Al_{0.48}Ga_{0.52}InP_2$ epilayer on glass (sample $G3$ in Table I). During data acquisition, the polarizer of the rotating-analyzer ellipsometer was fixed at $P = 45°$, i.e., the incident polarization state $\chi = \tan P$ in Eq. (14) is unity. The ellipsometric parameters are transformed into the pseudodielectric function $\langle \in \rangle$, which is a representation of Ψ and Δ assuming a two-phase model, for convenience.[41] The quality of the epilayer, after the wet-chemical removal of the GaAs substrate, is excellent (low surface roughness, high thickness uniformity). For photon energies below the lowest zone-center transition energies $E_0^{(1)}$, the real-valued film optical constants have slight dispersion, and multiple reflections occur between the film interfaces. Above $E_0^{(1)}$, the interference oscillations disappear due to the onset of absorption at this fundamental absorption edge. Except for $E_0^{(1)}$, the zone-center transition energies and strength parameters cannot be resolved from this data type. The $\Gamma_{6(1)v} - \Gamma_{6c}$, and $\Gamma_{6(2)v} - \Gamma_{6c}$ transitions are polarized almost parallel to the ordering direction, and mainly affect the extraordinary dielectric function $\in_{\parallel}$. The sensitivity of the standard ellipsometry parameters is limited to $\in = \frac{2}{3} \in_{\perp} + \frac{1}{3} \in_{\parallel}$. Further information about the sample anisotropy is required for analysis of the polarization-dependent E_0-type transitions. Nevertheless, beside $\in$, the thickness of the $Al_{0.48}Ga_{0.52}InP_2$ epilayer is obtained from this experiment. Standard ellipsometry parameters were also measured on the as-grown sample $A3$. Except for the thickness, which is slightly larger than that of the epilayer on glass, no further information is available from this data set.

B. Generalized ellipsometry

Figures 3 (Ψ_{sp}) and 4 (Δ_{sp}) show GVASE data measured in transmission (○; $\Phi_a = 0°$) and reflection (□; $\Phi_a = 15°$) on a CuPt-ordered $Al_{0.48}Ga_{0.52}InP_2$ epilayer on glass (sample $G3$). The insets enlarge the zone-center transition range. The data sets reveal most of the spectral features of the near-band-gap CuPt-order birefringence:

Below the first zone-center transition energy $E_0^{(1)}$, the birefringence is real valued and undergoes a sign change indicated by C. At this spectral position, the epilayer is isotropic, and both $\mathbf{t}_{sp}/\mathbf{t}_{ss}$ and $\mathbf{r}_{sp}/\mathbf{r}_{ss}$ vanish. Below C, the birefringence is positive, and pronounced interference oscillations occur in Ψ_{sp}. Above C, the order birefringence is negative with strong dispersion. At C, both $\Delta_{sp} = \arg(\mathbf{t}_{sp}/\mathbf{t}_{ss})$ and $\Delta_{sp} = \arg(\mathbf{r}_{sp}/\mathbf{r}_{ss})$ possess a reversal point.

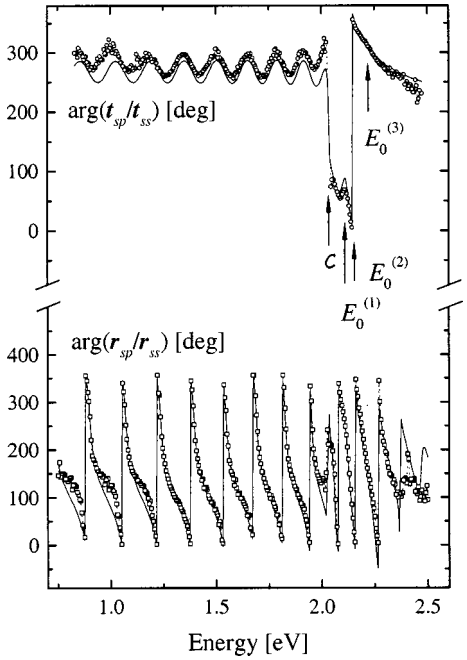

FIG. 4. Same as Fig. 3 for $\Delta_{sp}=\arg(\mathbf{t}_{sp}/\mathbf{t}_{ss})$ (○), and $\Delta_{sp}=\arg(\mathbf{r}_{sp}/\mathbf{r}_{ss})$ (□). The phase information provide sensitivity to the sign of the order birefringence, and, if necessary, to the in-plane orientation of the ordering direction φ during data acquisition.

The absorption of incident electric field polarization along the $(1\bar{1}\bar{1})$ sublattice planes entails the strong rise in $\Psi_{sp}=\tan^{-1}|\mathbf{t}_{sp}/\mathbf{t}_{ss}|$ at $E_0^{(1)}$. There, the reflection-type data are still dominated by interference effects. Both $\Delta_{sp}=\arg(\mathbf{t}_{sp}/\mathbf{t}_{ss})$ and $\Delta_{sp}=\arg(\mathbf{r}_{sp}/\mathbf{r}_{ss})$ possess another reversal point.

At $E_0^{(2)}$ the incident radiation polarized along the ordering direction excites electrons from the $\Gamma_{6(1)v}$ valence-band state to the Γ_{6c} conduction band state damping the p-s mode-coupled wave amplitudes for photon energies above $E_0^{(2)}$.

At $E_0^{(3)}$ the $\Gamma_{6(2)v}-\Gamma_{6c}$ transition is activated accompanied again by a change of dispersion of the birefringence. Above $E_0^{(3)}$ the epilayer becomes opaque. The transmission-type data pass into noise as the transmitted electric field intensities vanish. The exponential damping of the wave amplitudes reflected from the back side of the epilayer causes the decay of the interference oscillations within the reflection type data. Note that the $\Gamma_{6(2)v}-\Gamma_{6c}$ transition can be identified by the pronounced shoulders at $E_0^{(3)}$ in all data sets.

C. Dark-field spectroscopy

A photon-counting unit, attached to a home-made polarimetric experimental setup, was used to detect the cross-polarized transmission intensities $|\mathbf{t}_{sp}|^2$ of the same $Al_{0.48}Ga_{0.52}InP_2$/glass epilayer (sample $G3$). The upper panel of Fig. 5 shows the experimental (○) and best fit (——) DFS data. The inset enlarges the zone-center transition region. The spectral features observed here are similar to those for the transmission GVASE parameter Ψ_{sp}. However, the strong rise of the DFS signal at $E_0^{(1)}$ and the steep slope at $E_0^{(2)}$ form a unique lineshape which allows immediate identification of both transition energies. The ''spin-split'' transition $\Gamma_{6(2)v}-\Gamma_{6c}$ causes an asymmetric broadening of the DFS lineshape and a weak shoulder at $E_0^{(3)}$. The DFS signal vanishes also at C where the birefringence undergoes a sign change. Below C, multiple reflections within the transparent and birefringent film induce a similar interference pattern of p-s coupled modes as those which appear in Figs. 3 and 4.

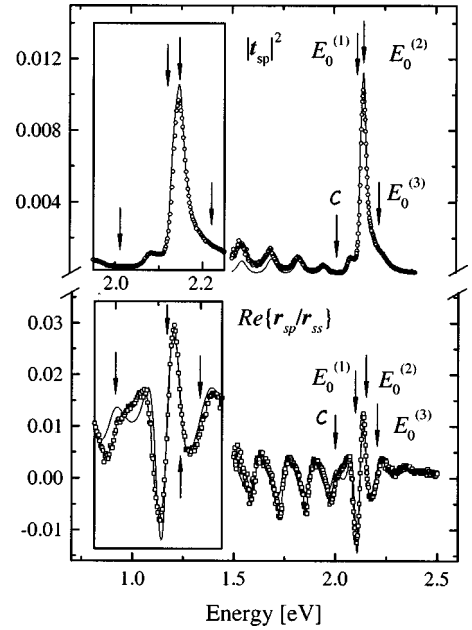

FIG. 5. DFS, i.e., $|\mathbf{t}_{sp}|^2$ (○; $\Phi_a=0°$, sample $G3$), and CRDS, i.e., $\mathrm{Re}\{\mathbf{r}_{sp}/\mathbf{r}_{ss}\}$ data (□; $\Phi_a=58°$, sample $A3$). The insets enlarge the zone-center transition region. The simulated data were calculated with the order-birefringence parameter obtained from simultaneous analysis of the GVASE, DFS, and CRDS data. The deviations between experimental and calculated CRDS data in the vincinity of C are attributed to surface-induced anisotropies.

D. Cross-polarized RDS

The lower panel of Fig. 5 shows the experimental (□) and best-fit (——) CRDS data from the as-grown $Al_{0.48}Ga_{0.52}InP_2$/GaAs sample $A3$ ($\Phi_a=58°$). The intensity sets in Eq. (20) were acquired for $\gamma=0.5°$, 1°, and 1.5°, and Eq. (20) resulted in similar values regardless of γ. (This behavior is expected as long as $\gamma\ll\pi/2$). The error bars on each individual CRDS data point were estimated to be less than 5%. The interference amplitudes below C are proportional to the absolute value of the order birefringence as expected from Eq. (21). At the isotropy point C, the slope of the interference oscillations is reversed due to the sign change in $\Delta\in$. Three reversal points above C indicate the zone-center transition energies where birefringent-interference, -absorption, and -dispersion effects overlap. Note that for isotropic surfaces, this modulation signal would be zero throughout regardless of the angle of incidence. The deviation between the experimental and best-fit data in the vicinity of C is attributed to surface-induced anisotropy.

Figure 6 shows the s to p polarized coefficients β_r and β_i for sample $A3$ (as-grown) calculated according to Eq. (B8) using $\in$ and d determined from the standard ellipsometry data. The calculated CRDS data shown in Fig. 5 are obtained using the order-birefringence parameters ($\Delta\in$ shown for η

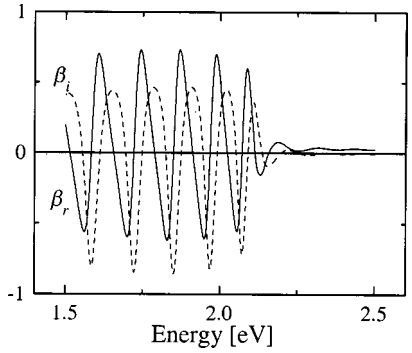

FIG. 6. Spectral dependence of the *s* to *p* polarized CRDS coefficients β_r (——) and β_i (– – –) calculated for an order-birefringent $Al_{0.48}Ga_{0.52}InP_2$ film on GaAs (sample *A*3).

$=0.47$ in Fig. 11) and the coefficients in Fig. 6. Below the band gap, the CRDS equals $\beta_r\ \Delta n^2$. Above the band gap, both real and imaginary parts of $\Delta\in$ contribute to the reflectance difference, and the CRDS data depend on the dispersion of the order-birefringence $\Delta\in$, the film thickness *d*, and $\in$. Excellent agreement is obtained between CRDS calculation and experiment, although the order-birefringence model ignores any nonparabolicity in the valence bands at $k\neq 0$.

E. CuPt-order birefringence

Figure 7 presents the major dielectric functions $\in_{\parallel}(\parallel[1\bar{1}1])$ and $\in_{\perp}(\perp[1\bar{1}1])$ in the near-band-gap spectral range of sample *A*3. The order-birefringence model from Sec. II is used for parameterization of $\in_{\parallel}$ and $\in_{\perp}$. All spectra shown in Figs. 2–5, and the standard ellipsometry data from the as-grown epilayer, were analyzed simultaneously. A 4×4 matrix formalism that accounts for plane-wave propagation in arbitrarily anisotropic layers was employed for the regression analysis (See also the appendix).[33] The multiple-data-type fits[34,42] were performed using a Levenberg-Marquardt regression algorithm[43] with an error function properly weighted to the estimated experimental errors.[45]

The angular in-plane (φ) and azimuth (Θ) orientations of the optical axis of the sample, i.e., the Euler angle φ and Θ which relate crystal and laboratory coordinate systems, were calculated according to the substrate miscut, and the sample alignment during GVASE, DFS, and CRDS data acquisition. The azimuth Θ is given in Table I, and represents the angle between the sample normal and the ordering direction. The in-plane orientation φ is the angle between the plane of incidence and the $[1\bar{1}0]$ direction, i.e., $\varphi=45°$.

Prior to parameterization of the order-birefringence in the near-band-gap region we determined the E_1 and E_2 critical-point contributions to the dispersion of the dielectric functions in this spectral range. We extended the spectral range for the GVASE measurements to 5 eV. We did not, however, observe appreciable sample anisotropy information. For photon energies above 2.5 eV, the ratios $\mathbf{R}_{ps}$ and $\mathbf{R}_{sp}$ are too small for resolution by this technique. The CRDS setup, which would be more powerful for detection of higher-energy critical point birefringence, was limited to photon energies of 3 eV. We therefore treated the E_1 and E_2 critical-point structures as isotropic, and no contributions were added

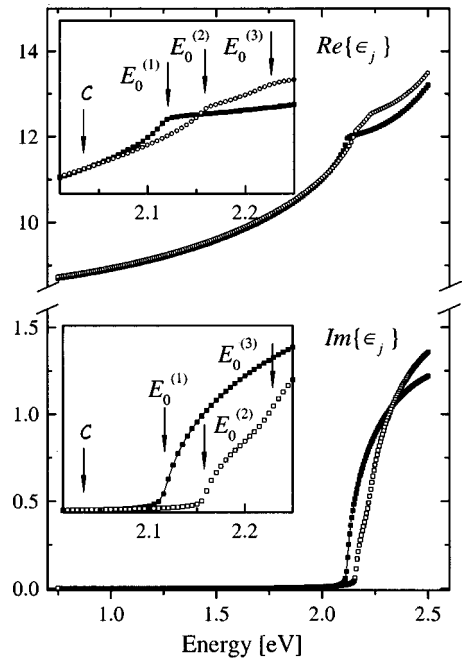

FIG. 7. Major dielectric function $\in_{\perp}$ (■), and $\in_{\parallel}$ (□) of CuPt-ordered $Al_{0.48}Ga_{0.52}InP_2$ (sample 3). The insets enlarge the zone-center transition range. Below the isotropy point *C*, the order birefringence is positive and real valued, and changes sign at *C*. Above the first zone-center transition $\Gamma_{4,5v}-\Gamma_{6c}(E_0^{(1)})$, the onset of absorption for polarizations perpendicular $[1\bar{1}1]$, and activation of the $\Gamma_{6(1)v}-\Gamma_{6c}$, and $\Gamma_{6(2)v}-\Gamma_{6c}$ transitions by polarizations parallel $[1\bar{1}1]$ cause strong dispersion in $\Delta\in=\frac{1}{3}\in_{\parallel}(\parallel[1\bar{1}1])-1/3\ \in_{\perp}(\perp[1\bar{1}1])$. The order birefringence allows simultaneous identification of the zone-center transitions of the CuPt-ordered alloy.

to the order-birefringence model. Instead, a harmonic oscillator was used to account for all higher-order critical point contributions to the near-band-gap dielectric function. We added, instead of the E_1 and E_2 CP's, a single DHO lineshape to both $\in_{\parallel}$ and $\in_{\perp}$ [Eq. (5); $A_2^{virt}=4.37$, $E_2^{virt}=3.66$ eV, $\Gamma_2^{virt}=0.0$ eV]. The order-birefringence model then comprises the zone-center transition contributions, the ''static'' dielectric constants $\in_{\parallel,\perp\infty}$, and the isotropic DHO dispersion.

The best-fit parameters of the experimental data from sample 3 to the order-birefringence model are given in Table II. The zone-center transition energies are marked by arrows in Fig. 7. As expected from the experimental data, the order birefringence is real-valued below $E_0^{(1)}$, and undergoes a sign change in *C* (see enlarged inset in Fig. 7). A positive but small birefringence remains then throughout the below-gap spectral range. This birefringence causes the interference pattern of *p*-*s* mode-coupled waves observed in all anisotropy data types. Above *C*, the lowest absorption edge at $E_0^{(1)}$ belongs to electric field polarization perpendicular to the ordering direction. The second ($E_0^{(2)}$) and third ($E_0^{(3)}$) absorption in this sample occurs mostly for plane wave polarization perpendicular to the ordered sublattice planes. We obtain that the $\Gamma_{6(1)v}-\Gamma_{6c}$, and $\Gamma_{6(2)v}-\Gamma_{6c}$ transitions are almost blocked for polarization perpendicular to the ordering direction. A second sign change of the real-part of $\Delta\in$ appears between the $\Gamma_{4,5v}-\Gamma_{6c}$ and $\Gamma_{6(1)v}-\Gamma_{6c}$ transitions. Note

TABLE II. Zone-center transition energies, strength, and broadening parameters obtained from the best fit of the order-birefringence model to the spectroscopic data. The $E_0^{(2)}$ and $E_0^{(3)}$ transitions are almost blocked for polarizations perpendicular to the ordering direction. The ''static'' dielectric constant $\epsilon_\infty=(2\epsilon_{\perp\infty}+\epsilon_{\parallel\infty})/3=4.174\pm0.02$ accommodates isotropic high-energy CP contributions not included within our model. The ''static'' contribution to the order-birefringence $\Delta\epsilon_\infty=(\epsilon_{\parallel\infty}-\epsilon_{\perp\infty})/3$ is influenced by ordering-induced splitting and shifting of all CP transitions. Up to now, it is unclear which of the critical points introduce positive or negative birefringence.

Sample i	$E_0^{(i)}$[eV] / $\Gamma_0^{(i)}$[meV] 1	2	3	$A_\perp^{(i)}$ / $A_\parallel^{(i)}$ 1	2	3	$\Delta\epsilon_\infty=(\epsilon_{\parallel\infty}-\epsilon_{\perp\infty})/3$
1	2.091±0.003	2.121±0.003	2.207±0.003	11.5	2.3	0.5	−0.115±0.018
	16±1	20±5	20±5	0.9	8.6	7.2	
2	2.101±0.001	2.129±0.003	2.212±0.003	11.4	1.2	1.4	−0.109±0.005
	10±1	11±1	14±2	0	8.3	7.1	
3	2.116±0.002	2.141±0.002	2.220±0.003	12.7	0	0.1	−0.108±0.005
	5±1	5±1	8±2	0.3	8.8	5.7	
4	2.139±0.001	2.159±0.002	2.234±0.003	12.8	0.3	2.3	−0.045±0.005
	9±2	6±1	25±2	0	11	5.9	

that, except for the redshift of the fundamental gap transition, the average dielectric function $\epsilon=\frac{2}{3}\epsilon_\perp+\frac{1}{3}\epsilon_\parallel$ is very similar to that obtained from random alloy samples reported recently (Ref. 44).

F. CuPt-order parameter

A series of $Al_{0.48}Ga_{0.52}InP_2$ samples (A: as-grown; G: on-glass) was investigated to study the influence of the degree of ordering on the order birefringence, and on the zone-center transition energies. Table I summarizes relevant sample structure parameters. Different substrate miscuts were included, and different degrees of ordering η were expected.[54] Spectroscopic data sets, as discussed above for sample 3, were acquired from all other samples. The experimental and best-fit data are shown in Figs. 8–10, and Fig. 13. (Presentation of the standard ellipsometry data is omitted).

Figures 8 and 9 present transmission and reflection GVASE data from samples $G1-G4$ (the spectra are shifted for clarity). All samples possess similar birefringence. However, the isotropy point C moves to higher energies, whereas the zone-center transitions are redshifted from bottom to top in Figs. 8 and 9. This redshift is well-known for ordered $GaInP_2$ or $AlInP_2$. Likewise, the valence-band splitting δE_{ij} increases. Figures 10 and 13 show experimental and best-fit DFS and CRDS data, respectively. Here, the shift of the peak-maximum at $E_0^{(2)}$, i.e., the $\Gamma_{6(1)v}-\Gamma_{6c}$ transition, is most obvious. The weak shoulder, as well, which emerges on the left side of the DFS signal, and which is caused by activation of the $\Gamma_{6(2)v}-\Gamma_{6c}$ transition, evolves into a pronounced structure from bottom to top in Fig. 10. The spectral position of this structure remains nearly unchanged, whereas the low-energy side of the DFS signal is shifted to longer wavelength.

Figure 11 presents refractive ($n_\parallel-n_\perp$; upper panel), and extinction coefficients ($k_\parallel-k_\perp$; lower panel) of the order-birefringence obtained from all samples ($\epsilon_{\parallel,\perp}=[n_{\parallel,\perp}+ik_{\parallel,\perp}]^2$). The order-birefringence model parameters are summarized in Table II. The transition energies, which result from the same best fit, were used to calculate the valence-band splitting values, which are plotted in Fig. 12 against the $\Gamma_{4,5v}-\Gamma_{6c}$ transition energy $E_0^{(1)}$. The dependencies of the three transition energies on $E_0^{(1)}$ can be explained by the quasicubic perturbation model, where the spin-orbit and crystal-field splitting parameters scale with the degree of ordering η, as described by Wei and Zunger [See Eqs. (6)–(11)

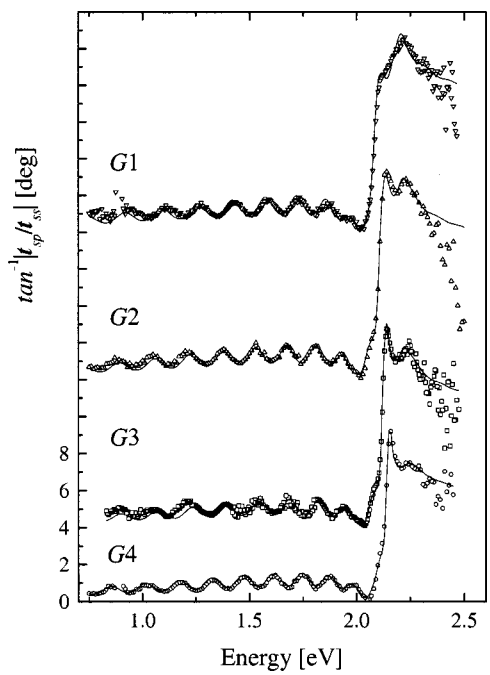

FIG. 8. Experimental (symbols) and best-fit (solid lines) transmission GVASE data (Ψ_{sp}) for a series of $Al_{0.48}Ga_{0.52}InP_2$ samples (epilayers on glass in Table I) with different degrees of ordering η. The spectra are shifted each by 8° for convenience. The lineshape within the zone-center transition region consists of a convolution of birefringent thickness interference and dispersion effects. The knowledge of the sample thickness is crucial for data analysis. η increases from bottom to top, as can be seen from the redshift of the steep flank ($E_0^{(1)}$ position) above the zero point where the order-birefringence changes sign, and the $E_0^{(2)}$ peak positions (see also Fig. 3).

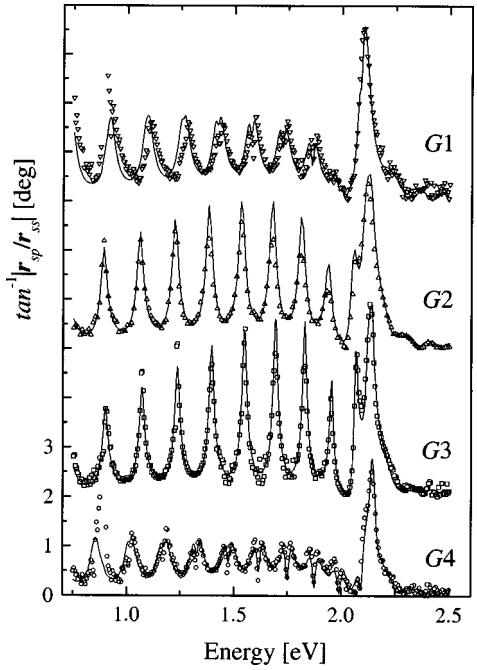

FIG. 9. Same as Fig. 8 for the reflection GVASE parameter $\Psi_{sp}=\tan^{-1}|\mathbf{r}_{sp}/\mathbf{r}_{ss}|$ ($\Phi_a=15°$). The spectra are shifted each by 3° for convenience.

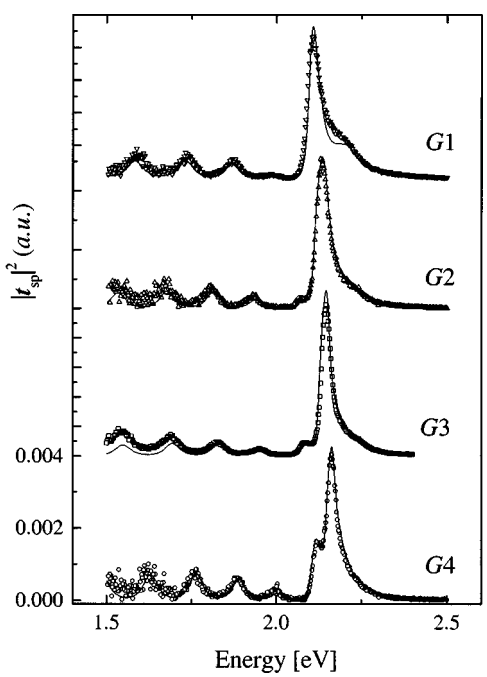

FIG. 10. Same as Fig. 8 for the DFS data. The spectra are shifted for convenience. Note the shoulder on the high-energy side of the DF spectra which becomes more pronounced as η increases (from bottom to top). This shoulder is caused by the change of dispersion of the order birefringence upon activation of the third zone-center transition at $E_0^{(3)}$. The small side band on the left of the DFS signal is caused by interference oscillations which overlap the strong-rise signal at $E_0^{(1)}$ (see also Fig. 5). A lineshape analysis is necessary to identify all zone-center transitions securely.

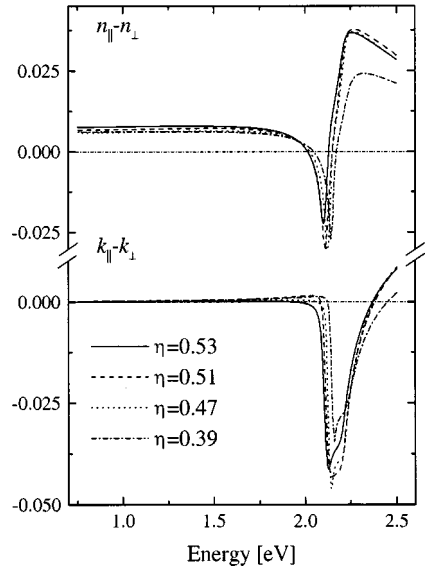

FIG. 11. Order birefringence of spontaneously CuPt-ordered $Al_{0.48}Ga_{0.52}InP_2$ with different degrees of ordering η (Table I). The birefringence undergoes two sign changes, below and within the zone-center transitions. Below the band-gap, the birefringence is positive and scales with η. The successive activation of the zone-center transitions cause strong dispersion changes. The order parameters are estimated after Wei and Zunger (Ref. 6; see also captions in Table I).

in Sec. II].[7] The dotted lines in Fig. 12 represent the best fit of the experimentally determined transition energies to the quasicubic perturbation parameters. We obtain

$$\Delta_{\rm so}^{(\eta=0)}=78\pm5\ \text{meV},\qquad E_g^{(\eta=0)}=2.195\pm0.005\ \text{eV},$$

$$\zeta^{-1}=\delta\Delta_{\rm so}^{(\eta=1)}/\Delta E_g^{(\eta=1)}=0.0\pm0.1,$$

and

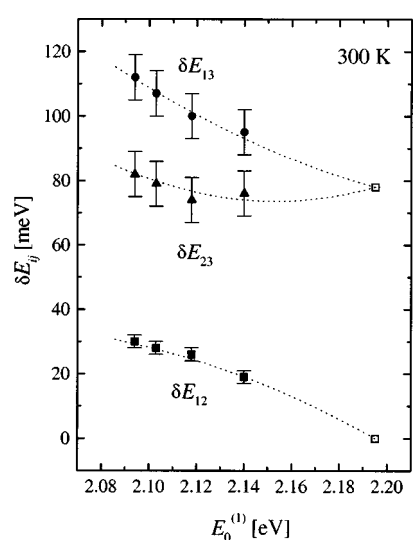

FIG. 12. Valence-band splittings δE_{ij} (symbols) for $Al_{0.48}Ga_{0.52}InP_2$ with different degrees of ordering at 300 K plotted against $E_0^{(1)}$. The dotted lines represent the best fit after Wei, Laks, and Zunger (Ref. 6), and parameters $\Delta_{\rm SO}^{(\eta=0)}$, $\Delta_{\rm CF}^{(\eta=0)}$, $E_g^{(\eta=0)}$, $\delta\Delta_{\rm SO}^{(\eta=1)}/\Delta E_g^{(\eta=1)}$, and $\delta\Delta_{\rm CF}^{(\eta=1)}/\Delta E_g^{(\eta=1)}$ given in Table III.

TABLE III. Quasicubic model parameters for CuPt-ordered $Al_{0.48}Ga_{0.52}InP_2$. The spin-orbit splitting parameter found here is nearly ordering independent.

	$Al_xGa_{1-x}InP_2$ ($x=0.48$)	
	Present work	Reference
$E_g^{(\eta=0)}$ [eV]	2.195 ± 0.005	2.199[a]
		2.176[b]
		2.212[c]
$\Delta_{SO}^{(\eta=0)}$ [meV]	78 ± 5	92[d]
$\delta\Delta_{SO}^{(\eta=1)}/\Delta E_g^{(\eta=1)}$	0 ± 0.05	0.048[e]
$\delta\Delta_{CF}^{(\eta=1)}/\Delta E_g^{(\eta=1)}$	0.620 ± 0.02	0.620[e]

[a]E_g [eV]$=1.9+0.57x+0.11x^2$, Ref. 46.
[b]E_g [eV]$=1.89+0.51x+0.18x^2$, Ref. 47.
[c]E_g [eV]$=1.885+0.681x$, Ref. 48.
[d]Averaged between the Γ_{8v} and Γ_{7v} states of GaP, InP, and AlP taken from Wei and Zunger (Table II in Ref. 7), according to the volume fractions of the binaries in the $Al_{0.48}Ga_{0.52}InP_2$ alloy.
[e]Linear interpolation between $GaInP_2$ and $AlInP_2$ calculated by Wei and Zunger (Ref. 7).

$$\xi^{-1}=\delta\Delta_{CF}^{(\eta=1)}/\Delta E_g^{(\eta=1)}=0.62\pm0.02.$$

(The crystal-field splitting of the random alloy $\Delta_{CF}^{(\eta=0)}$ is zero.) For different degrees of ordering η, the valence-band splitting energies are mostly influenced by the change of the crystal-field splitting parameter. The spin-orbit splitting parameter remains nearly constant for the ordered and disordered compound ($\delta\Delta_{so}=0$). Table III compares the best-fit parameters with available theoretical (Δ_{so}, ζ, ξ) and experimental ($E_g^{(\eta=0)}$) data for the $Al_{0.48}Ga_{0.52}InP_2$ alloy. Excellent agreement is obtained between the linear interpolation of recently predicted values for $AlInP_2$ and $GaInP_2$ (Wei and Zunger, Ref. 7).

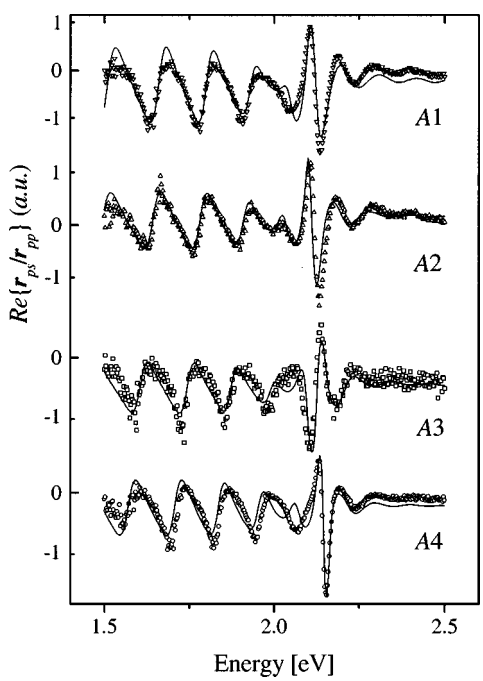

FIG. 13. Experimental (symbols) and best-fit (solid lines) CRDS data ($\mathrm{Re}\{\mathbf{r}_{sp}/\mathbf{r}_{ss}\}$, $\Phi_a=58°$) for the as-grown $Al_{0.48}Ga_{0.52}InP_2$ samples listed in Table I. The calculated data were obtained using the order-birefringence model parameter, derived during the analysis of the ellipsometry-type and DFS data, without further parameter variation, resulting in good agreement between theory and experiment.

V. DISCUSSION

Dispersion and sign change of the order birefringence for photon energies below $E_0^{(1)}$ have been already found by Wirth *et al.* in ordered $GaInP_2$ and $Al_{0.33}Ga_{0.67}InP_2$ (Fig. 8 in Ref. 15). There, the authors investigated the supermode orientation in planar waveguide structures, and found that ordered $Al_yGa_{1-y}InP_2$ ($y=0$, 0.33) is positively birefringent far below the band gap, and negatively birefringent when approaching the band gap. Unfortunately, the authors could not extend their investigations for wavelength close to, or above the band gap because of the strong absorption of the guided waves in this spectral range. A six-band *kp* method for ordered $Al_yGa_{1-y}InP_2$ was used to calculate the order birefringence below the band gap. The *kp* method resulted in the correct dispersion, but failed to explain the isotropy point and sign change in Δn. The latter was attributed to high-energy CP contributions which possibly induces long-tail birefringence within the below-gap spectral range. Recently, Wirth *et al.* also observed the same type of birefringence in CuPt-ordered $GaInAs_2$.[20,21] It appears that the order birefringence observed so far is inherent to the CuPt-ordered state in the $Al_yGa_{1-y}InP_2$ system regardless of the composition x. Furthermore, it is likely that the same order birefringence may be found throughout the $Al_yGa_{1-y}InAs_2$ system as well.

Luo *et al.* measured RDS features on ordered $GaInP_2$ samples acquiring reflectance for polarization parallel $[1\bar{1}0](R_{[1\bar{1}0]})$ and $[110](R_{[110]})$. The authors used a 4×4 Luttinger model for calculation of RDS features of ordered $GaInP_2$, neglecting coupling with the spin-orbit split-off band.[17] More recently, Luo *et al.* extended their calculations by a *k*-dependent eight-band model.[18] Beside the ordering-induced coupling of the crystal-field and spin-orbit split-off band, this model includes the *k* dependence of the transition matrix elements. Wei and Zunger have presented a similar theory for RDS in CuPt-ordered III-V compounds using a six-band model treating coupling with the spin-orbit split-off band, but neglecting the transition matrix *k* dependence.[49] Figure 2 in Ref. 18 compares the resulting lineshapes from the four-band, six-band, and *k*-dependent eight-band model. Although some improvement was obtained from the *k*-dependent eight-band model, the agreement between the experimental RD spectrum and the calculation there is still unsatisfactory. Nevertheless, the authors argue that the order-induced coupling between the three valence bands at $k\neq0$ cannot be neglected for correct RDS data analysis.

Because of the discrepancy concerning the necessity of treating nonparabolicity of the valence bands, we also performed standard RDS measurements at near-normal incidence ($\Phi_a=4°$) on sample 3. Figure 14 shows experimental (□) and calculated (——) data. The RDS data are very similar to the CRDS data (both techniques sense the same sample anisotropy). The calculated RD spectrum in Fig. 14 is obtained using Eq. (B14), and the order-birefringence model

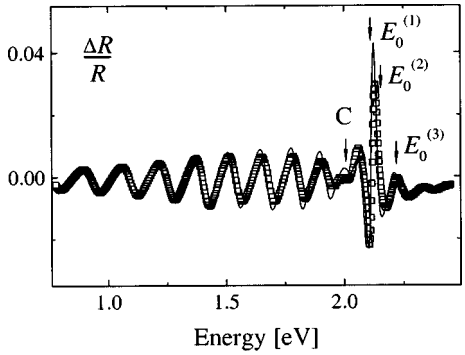

FIG. 14. Experimental (symbols) and best-fit (solid lines) RDS data ($\Phi_a = 4°$) for the as-grown $Al_{0.48}Ga_{0.52}InP_2$ sample 3 in Table I. The calculated data were obtained using the order-birefringence model without further parameter variation, resulting in excellent agreement between theory and experiment.

parameters for sample $A3$ without further parameter variation. The order-birefringence model established in this work obviously fits the RDS data as well. The theories presented by Wei and Zunger,[49] and Luo *et al.*[18] for analysis of RD spectra of CuPt-ordered compounds, neglect *p-s* mode coupling effects due to wave amplitudes reflected from the film-substrate interface, i.e., bulk reflectivity equations are used for analysis of the experiment. We therefore conclude that (i) the treatment of k dependence of the transition matrix elements within the CuPt-order birefringence model is avoidable, (ii) the piezobirefringence model, i.e., the parabolic band approximations suffice for calculation of the near-band-gap dispersion of the CuPt-ordered dielectric function tensor, and (iii) correct treatment of plane wave propagation in birefringent thin films is crucial for correct analysis of polarization-dependent spectroscopy data. We therefore added the appendix to the present work that includes explicit expressions for all data types used here.

VI. CONCLUSIONS

To summarize, we have presented a consistent approach to quantify the order-induced birefringence in the near-band-gap spectral range (0.75 to 2.5 eV) for spontaneously ordered $Al_{0.48}Ga_{0.52}InP_2$. Four different experimental techniques: generalized ellipsometry, dark-field spectroscopy, cross-polarized, and standard reflectance difference spectroscopy were used simultaneously for determination of the sample dielectric function tensor. The observed order birefringence is treated as ''chemical-stress'' induced piezobirefringence. The dielectric function model for piezobirefringence in zinc-blende compounds, and selection rules for the transitions from the $\Gamma_{4,5v}, \Gamma_{6(1)v}, \Gamma_{6(2)v}$ valence band states to the Γ_{6c} conduction band states, suffice for calculation of the order birefringence in the near-band-gap spectral region. It was shown that explicit treatment of the transition-matrix k dependence, as recently suggested for ordered $GaInP_2$ or $GaInAs_2$, is unnecessary. Instead, consideration of multiple internal reflections within the thin-film samples results in improved data analysis. The transition energies, strengths, and broadening parameters for the three zone-center transitions are obtained from parameterization of the sample dielectric function tensor. The quasicubic perturbation parameters are obtained for $Al_{0.48}Ga_{0.52}InP_2$ in excellent consistency with recent theoretical predictions by Wei and Zunger. We find, almost ordering independent, the spin-orbit splitting parameter of 76 meV, and the crystal-field splitting band-gap reduction ratio for the perfectly ordered alloy of 0.62. The band gap of the random alloy is 2.195 eV. A cross-polarized reflectance difference technique was further introduced to sense the extremely weak anisotropy in as-grown CuPt-type ordered samples at oblique angles of incidence. This technique is nondestructive, and avoids removal of the substrate material. Equations for light propagation in CuPt-type ordered thin-film samples according to each experimental data type used in this work are given in the appendix.

ACKNOWLEDGMENTS

M.S. wishes to express his gratitude to Ralf Wirth at University Stuttgart for helpful collaboration, and for providing the RDS data. We thank B. Haase and H. Herrenberger for their patience during sample preparation. We gratefully acknowledge helpful discussions with G. Benndorf and Professor R. Schwabe and Professor K. Kreher, University Leipzig. M.S. also thanks Craig M. Herzinger and Blaine Johs at J. A. Woollam Co. for providing the GVASE acquisition routines. This work was supported by the Deutsche Forschungsgemeinschaft under Project No. Rh. 28/1-1,2.

APPENDIX A: T_p FOR CuPt-ORDERED THIN FILMS

The 4×4 matrix formalism is employed for calculation of the GVASE, CRDS, RDS, and DFS data types for CuPt-ordered thin films. This approach accounts self-consistently for multiple internal reflections within the order-birefringent film. All equations are derived to first order approximation in $\Delta\epsilon$, i.e., $\|\Delta\epsilon\| \ll \|\epsilon\|$ is assumed throughout, and second- or higher-order terms in $\Delta\epsilon$ are omitted. The inclination Θ of the ordering direction from the sample normal amounts to $\cos^{-1}(1/\sqrt{3})$ for (001) surfaces. This assumption is still a good approximation for (100) samples with miscuts not greater than 6°. The approximate equations given below were compared to results using exact solutions for light propagation in arbitrary anisotropic thin-film samples presented previously.[33] For values of $\Delta\epsilon$ measured in this work, both the approximate equations and the exact solutions provide the same numerical values. The approximations presented here can be used for immediate and straightforward data analysis, and may shed light on spectral features due to CuPt-order-induced birefringence in III-V-semiconductor compounds observed by polarization-dependent techniques.

For the framework of the 4×4 matrix formalism, the symbols, and the coordinate system used here, the reader is referred to Refs. 31, 33, 35, 50, and references therein. To begin with here, the partial transfer matrix $\mathbf{T}_p$ for a thin film of CuPt-ordered alloy is derived for two typical sample arrangements (the RDS setup and the CRDS setup). The GVASE, DFS, CRDS, and RDS equations are then obtained using ambient and substrate matrices for computation of the anisotropic Jones reflection and transmission coefficients. (See Appendix B.)

(i) $[100]\|x$ (CRDS setup): Without loss of generality the

$[1\bar{1}1]$ direction is chosen as stacking direction of {111} sublattice planes that form the CuPt structure within the zinc-blende alloy (Fig. 1). For the experiment the sample is aligned such that the [100] direction is parallel to the x axis of the laboratory coordinate system, and hence parallel to the plane of incidence. At the same time, the $[1\bar{1}0]$ direction, which is parallel to the sample surface, is rotated away from the plane of incidence by $\varphi=\pi/4$. The dielectric function tensor $\hat{\epsilon}$ in laboratory coordinates is then expressed as follows $[\Theta=\cos^{-1}(1/\sqrt{3})\sim 54.7°]$:

$$\hat{\epsilon}=\begin{pmatrix} \epsilon & -\Delta\epsilon & \Delta\epsilon \\ -\Delta\epsilon & \epsilon & -\Delta\epsilon \\ \Delta\epsilon & -\Delta\epsilon & \epsilon \end{pmatrix}, \tag{A1}$$

where $\Delta\epsilon=\frac{1}{3}\epsilon_{\parallel}-\frac{1}{3}\epsilon_{\perp}$, $\epsilon=\frac{1}{3}\epsilon_{\parallel}+\frac{2}{3}\epsilon_{\perp}$, and $\epsilon_{\parallel},\epsilon_{\perp}$ refer to the dielectric functions for polarizations parallel or perpendicular to the ordering direction, respectively. Berreman introduced the coefficient matrix $\hat{\Delta}$ of the first-order Maxwell differential equation system for light propagation through anisotropic media with plane parallel interfaces.[50] For the CuPt-ordered alloy, the complex rank-4 wave transfer matrix $\hat{\Delta}$ implies

$$\hat{\Delta}=\frac{1}{\epsilon}\begin{pmatrix} -k_x\Delta\epsilon & k_x\Delta\epsilon & 0 & \epsilon-k_x^2 \\ 0 & 0 & -\epsilon & 0 \\ \epsilon\Delta\epsilon & -\epsilon(\epsilon-k_x^2) & 0 & -k_x\Delta\epsilon \\ \epsilon^2 & -\epsilon\Delta\epsilon & 0 & -k_x\Delta\epsilon \end{pmatrix}. \tag{A2}$$

The x component of the incident wave vector $k_x=n_a\sin\Phi_a$ depends on the ambient index of refraction n_a and the angle of incidence Φ_a. The eigenvalues of $\hat{\Delta}$ are $q_{1,2}=\pm\sqrt{(\epsilon-k_x^2-\Delta\epsilon)}$, and $q_{3,4}=-k_x\Delta\epsilon/\epsilon\pm\sqrt{(\epsilon-k_x^2+\Delta\epsilon)}$. We define $q^2=\epsilon-k_x^2$, and decompose $\hat{\Delta}$ into $\hat{D}+(\Delta\epsilon)\hat{\delta}$ using

$$\hat{\mathbf{D}}=\begin{bmatrix} 0 & 0 & 0 & \frac{q^2}{\epsilon} \\ 0 & 0 & -1 & 0 \\ 0 & -q^2 & 0 & 0 \\ \epsilon & 0 & 0 & 0 \end{bmatrix},$$

$$\hat{\delta}=\frac{1}{\epsilon}\begin{pmatrix} -k_x & k_x & 0 & 0 \\ 0 & 0 & 0 & 0 \\ \epsilon & 0 & 0 & -k_x \\ 0 & -\epsilon & 0 & -k_x \end{pmatrix}. \tag{A3}$$

The matrix $\mathbf{T}_p$ constitutes the solution of the Maxwell first-order differential equation system for plane parallel interfaces. The complex rank-4 matrix describes coupling and propagation of electromagnetic plane waves across a homogeneous birefringent film with thickness d.[50] $\mathbf{T}_p$ can be calculated as finite series expansion in $\hat{\Delta}$:[51,52]

$$\mathbf{T}_p\equiv\exp\{-ik_0\hat{\mathbf{\Delta}}d\}=\gamma_0\hat{\mathbf{E}}+\gamma_1\hat{\mathbf{\Delta}}+\gamma_2\hat{\mathbf{\Delta}}^2+\gamma_3\hat{\mathbf{\Delta}}^3, \tag{A4}$$

where $k_0=\omega/c$, ω and c are the angular light frequency and the vacuum light velocity, respectively, and $\hat{\mathbf{E}}$ is the unit matrix. The scalars γ_i follow from the eigenvalues q_i of $\hat{\Delta}$, and do not depend on $\Delta\epsilon$:

$$\gamma_0=\cos(k_0dq)-\frac{1}{2}k_0dq\sin(k_0dq),$$

$$\gamma_1=(i/2q)\{-k_0dq\cos(k_0dq)-3\sin(k_0dq)\},$$

$$\gamma_2=(1/2q^2)k_0dq\sin(k_0dq),$$

$$\gamma_3=(i/2q^3)\{k_0dq\cos(k_0dq)+\sin(k_0dq)\}. \tag{A5}$$

$\mathbf{T}_p$ decomposes into $\hat{\mathbf{I}}+\Delta\epsilon\hat{\mathbf{B}}$ with

$$\hat{\mathbf{I}}=\hat{\mathbf{E}}\cos(k_0dq)-\frac{i}{q}\hat{\mathbf{D}}\sin(k_0dq), \tag{A6}$$

$$\hat{\mathbf{B}}=(\gamma_1+2q^2\gamma_3)\hat{\boldsymbol{\delta}}+\gamma_2\hat{\boldsymbol{\gamma}}+\gamma_3\hat{\boldsymbol{\sigma}}, \tag{A7}$$

and $\hat{\gamma}=\hat{\mathbf{D}}\hat{\delta}+\hat{\delta}\hat{\mathbf{D}}$, $\hat{\sigma}=\hat{\mathbf{D}}\hat{\delta}\hat{\mathbf{D}}$, which results in

$$\hat{\boldsymbol{\gamma}}=\begin{pmatrix} 0 & -\frac{q^2}{\epsilon} & -\frac{k_x}{\epsilon} & -2k_x\frac{q^2}{\epsilon^2} \\ -1 & 0 & 0 & \frac{k_x}{\epsilon} \\ -k_x & 0 & 0 & \frac{q^2}{\epsilon} \\ -2k_x & k_x & 1 & 0 \end{pmatrix},$$

$$\hat{\boldsymbol{\sigma}}=\begin{pmatrix} -k_x\frac{q^2}{\epsilon} & 0 & \frac{q^2}{\epsilon} & 0 \\ k_x & 0 & 0 & -\frac{q^2}{\epsilon} \\ 0 & 0 & 0 & 0 \\ 0 & 0 & -k_x & -k_x\frac{q^2}{\epsilon} \end{pmatrix}. \tag{A8}$$

The identities $\hat{\mathbf{D}}^2=q^2\hat{\mathbf{E}}$, $\hat{\mathbf{D}}^3=q^2\hat{\mathbf{D}}$ are used. Note that $T_{p22}=\hat{I}_{22}$, $T_{p23}=\hat{I}_{23}$, $T_{p32}=\hat{I}_{32}$, and $T_{p33}=\hat{I}_{33}$ do not depend on $\Delta\epsilon$. T_{p11}, T_{p14}, T_{p41}, and T_{p44} are of type $T_{pij}=\hat{I}_{ij}+\Delta\epsilon\hat{B}_{ij}$, whereas the remaining elements $T_{pij}=\Delta\epsilon\hat{B}_{ij}$ are linear in $\Delta\epsilon$.

(ii) $[1\bar{1}1]\parallel(x\text{-}z)$ plane (RDS setup): For RDS experiments the sample is commonly aligned such that the $[1\bar{1}1]$ direction is within the $(x\text{-}z)$ plane. The $(x\text{-}z)$ plane is identical with the plane of incidence. The dielectric function tensor $\hat{\epsilon}$ in laboratory coordinates then reads

$$\hat{\epsilon}=\begin{pmatrix} \epsilon+\Delta\epsilon & 0 & \sqrt{2}\Delta\epsilon \\ 0 & \epsilon-\Delta\epsilon & 0 \\ \sqrt{2}\Delta\epsilon & 0 & \epsilon \end{pmatrix}. \tag{A9}$$

The derivation of $\mathbf{T}_p$ follows the same line as given above. The coefficients γ_i and the matrix $\hat{\mathbf{I}}$ are the same as in Eqs. (A5) and (A6), respectively. The elements of $\hat{\delta}$, $\hat{\gamma}$, and $\hat{\sigma}$ are $\delta_{11}=\delta_{44}=-\sqrt{2}k_x/\in$, $\delta_{32}=\delta_{41}=1$ (other $\delta_{ij}=0$); $\gamma_{11}=\gamma_{44}=q^2/\in$, $\gamma_{14}=q^2/\in^2\gamma_{41}$, $\gamma_{41}=-2\sqrt{2}k_x$, $\gamma_{22}=\gamma_{33}=-1$; $\sigma_{11}=\sigma_{44}=-\sqrt{2}k_x\gamma_{11}$, $\sigma_{14}=\gamma_{11}^2$, $\sigma_{23}=1$ (other $\gamma_{ij}=\sigma_{ij}=0$). A similar setup used for RDS experiments is where the ordering direction lies within the (y-z) plane. $\mathbf{T}_p$ can be decomposed in the same way, but, for the oblique angle of light incidence, the resulting expressions differ slightly from those given above. Both orientations, $[1\bar{1}\bar{1}]\|(y\text{-}z)$ and $[1\bar{1}1]\|(x\text{-}z)$, are not equivalent to each other with respect to the light propagation through birefringent thin films. Sometimes these two orientations are used for data acquisition to cancel out systematic errors by averaging the data sets. This fact may then find consideration.

APPENDIX B: GVASE, DFS, CRDS, AND RDS EQUATIONS

The concept of the 4×4 matrix algebra provides the matrix $\mathbf{T}$ from which the complex reflection and transmission elements are computed.[53] For a single CuPt-ordered film on an isotropic substrate $\mathbf{T}=\mathbf{L}_a^{-1}\mathbf{T}_p\mathbf{L}_f$, where $\mathbf{L}_a$ and $\mathbf{L}_f$ account for the optical properties of the ambient ($\in_a=n_a^2$), and the substrate ($\in_f=n_f^2$) materials, respectively. Derivation of $\mathbf{L}_a$ and $\mathbf{L}_f$ is given in Ref. 33. The matrix multiplication yields nonvanishing elements in the first and third column of $\mathbf{T}$ only:

$$T_{11}=[T_{p22}-T_{p23}N_{ff}]-[T_{p32}-T_{p33}N_{ff}]/N_{aa},$$

$$T_{21}=[T_{p22}-T_{p23}N_{ff}]+[T_{p32}-T_{p33}N_{ff}]/N_{aa},$$

$$T_{31}=[T_{p42}-T_{p43}N_{ff}]/n_a+[T_{p12}-T_{p13}N_{ff}]/\cos\Phi_a,$$

$$T_{41}=[T_{p42}-T_{p43}N_{ff}]/n_a-[T_{p12}-T_{p13}N_{ff}]/\cos\Phi, \tag{B1}$$

$$T_{13}=[T_{p21}\cos\Phi_f+T_{p24}n_f]-[T_{p31}\cos\Phi_f+T_{p34}n_f]/N_{aa},$$

$$T_{23}=[T_{p21}\cos\Phi_f+T_{p24}n_f]+[T_{p31}\cos\Phi_f+T_{p34}n_f]/N_{aa},$$

$$T_{33}=[T_{p41}\cos\Phi_f+T_{p44}n_f]/n_a+[T_{p11}\cos\Phi_f+T_{p14}n_f]/\cos\Phi_a,$$

$$T_{43}=[T_{p41}\cos\Phi_f+T_{p44}n_f]/n_a-[T_{p11}\cos\Phi_f+T_{p14}n_f]/\cos\Phi_a, \tag{B2}$$

with

$$N_{ij}\equiv n_i\cos\Phi_j=n_i\sqrt{1-[(n_a/n_j)\sin\Phi_a]^2}. \tag{B3}$$

In the following, the elements of T are labeled as T'_{ij} if we set $T_{pij}=\hat{I}_{ij}$, and T''_{ij} if we set $T_{pij}=\hat{B}_{ij}$.

(i) $[100]\|x$ (GVASE, CRDS, and DFS): It follows from $\mathbf{T}_p$ that T_{11} and T_{21} do not depend on $\Delta\in$, whereas T_{31}, T_{41}, T_{13}, and T_{23} are proportional to $\Delta\in$. The elements T_{33} and T_{43} are of the type $a+b\Delta\in$. The GVASE ratios $\mathbf{R}_{ps}$, $\mathbf{R}_{sp}$, and $\mathbf{R}_{pp}$ follow from $\mathbf{T}$:[53,33,35]

$$R_{ps}=\frac{T_{11}T_{23}-T_{21}T_{13}}{T_{11}T_{43}-T_{41}T_{13}},\quad R_{sp}=\frac{T_{41}T_{33}-T_{43}T_{31}}{T_{21}T_{33}-T_{23}T_{31}},$$

and

$$R_{pp}=\frac{T_{11}T_{43}-T_{41}T_{13}}{T_{21}T_{33}-T_{23}T_{31}}. \tag{B4}$$

The ratios are expanded according to

$$[c/(a+b\Delta\in)]\Delta\in\sim(c/a)\Delta\in,$$

or

$$[(A+\Delta\in B)/(C+\Delta\in D)]\sim(A/C)+\Delta\in[B/C-(A/C)\times(D/C)].$$

This allows factorization of $\mathbf{R}_{ps}$, $\mathbf{R}_{sp}$, and $\mathbf{R}_{pp}$ into

$$R_{ps;sp}=\Delta\in(\beta_r+i\beta_i)_{ps;sp}+O((\Delta\in)^2), \tag{B5}$$

$$R_{pp}=(\mathbf{r}_p/\mathbf{r}_s)[1+\Delta\in(\beta_r+i\beta_i)_{pp}+O((\Delta\in)^2)], \tag{B6}$$

with the coefficients β_r and β_i:

$$(\beta_r+i\beta_i)_{ps}=T''_{23}/T'_{43}-\mathbf{r}_sT''_{13}/T'_{43}, \tag{B7}$$

$$(\beta_r+i\beta_i)_{sp}=T''_{41}/T'_{21}-\mathbf{r}_pT''_{31}/T'_{21}, \tag{B8}$$

$$(\beta_r+i\beta_i)_{pp}=T''_{43}/T'_{43}-T''_{33}/T'_{33}. \tag{B9}$$

The isotropic ratios $\mathbf{r}_p$ and $\mathbf{r}_s$ are those for the complex p and s polarized reflectance of an isotropic ambient-film-substrate system with $\in$ being the dielectric constant of the film.[30] The experimental p-s and s-p polarized CRDS data types follow from the real parts of Eqs. (B7) and (B8), respectively. Note that the generalized ellipsometric ratio $\mathbf{R}_{pp}$ evolves from $\mathbf{r}_p/\mathbf{r}_s$, and determines $\in$. The ratios $\mathbf{R}_{ps}$ and $\mathbf{R}_{sp}$ are sensitive to $\Delta\in$, but still depend on $\in$. Only simultaneous analysis of all GVASE parameters can provide both $\in$ and $\Delta\in$ unambiguously.

The DFS data type is proportional to $|\mathbf{t}_{sp}|^2$. (Note that at normal incidence, $\mathbf{t}_{sp}=\mathbf{t}_{ps}$.) The cross-polarized transmission coefficient $\mathbf{t}_{sp}$ follows from $\mathbf{T}$:[33,35,53]

$$t_{sp}=\frac{-T_{13}}{T_{11}T_{33}-T_{13}T_{31}}. \tag{B10}$$

$\mathbf{t}_{sp}$ is expanded according to $[c/(a+b\Delta\in)]\Delta\in\sim(c/a)\Delta\in$. This allows factorization of $|\mathbf{t}_{sp}|^2$ into

$$|t_{sp}|^2=\|\Delta\in\|\|\alpha_r+i\alpha_i\|+O(\|\Delta\in\|^2), \tag{B11}$$

where $\|a\|$ denotes aa^*, and the star denotes the complex conjugate. Note that the DFS data are proportional to the square of $\Delta\in$. The coefficients α_r and α_i are

$$(\alpha_r+i\alpha_i)_{ps}=T''_{13}/(T'_{11}T'_{33}). \tag{B12}$$

(ii) $[1\bar{1}\bar{1}]\|(y\text{-}z)$ plane (RDS): Here, T_{31}, T_{41}, T_{13}, and T_{23} are zero, $T_{11},T_{21},T_{33},T_{43}$ are of the generic type $a+b\Delta\in$. The RD signal is defined by the weighted differ-

ence between the p to p and s to s polarized reflection coefficients $\mathbf{r}_{pp}$ and $\mathbf{r}_{ss}$, respectively. Those follow accordingly from $\mathbf{T}$:[33,35,53]

$$\frac{\Delta R}{R}=2\frac{\|T_{11}T_{43}-T_{41}T_{13}\|-\|T_{21}T_{33}-T_{23}T_{31}\|}{\|T_{11}T_{43}-T_{41}T_{13}\|+\|T_{21}T_{33}-T_{23}T_{31}\|}, \quad \text{(B13)}$$

where $\|a\|$ denotes aa^*. Expansion of numerator and denominator yields

$$\frac{\Delta R}{R}=\left[\frac{\Delta R}{R}\right]_{is}+\mathrm{Re}\{\Delta\in(\beta_r+i\beta_i)\}+O[(\Delta\in)^2], \quad \text{(B14)}$$

with

$$(\beta_r+i\beta_i)=2(\tan^2\Psi+1)^{-1}\left\{\tan^2\Psi\left(\frac{T''_{11}}{T'_{11}}+\frac{T''_{43}}{T'_{43}}\right)\times\left[2-\left[\frac{\Delta R}{R}\right]_{is}\right]-\left(\frac{T''_{21}}{T'_{21}}+\frac{T''_{33}}{T'_{33}}\right)\left[2+\left[\frac{\Delta R}{R}\right]_{is}\right]\right\}. \quad \text{(B15)}$$

The isotropic terms $\Delta R^{is}/R=(\|\mathbf{r}_p\|-\|\mathbf{r}_s\|)/(\|\mathbf{r}_p\|+\|\mathbf{r}_s\|)$ and $\tan^2\Psi=\|\mathbf{r}_p\|/\|\mathbf{r}_s\|$ refer to the isotropic three-phase model.[30] $\Delta R^{is}/R$ and Ψ depend on d, $\in$, and Φ_a. At normal incidence ($\Phi_a=0$) $\Delta R^{is}/R=0$ and $\tan\Psi=1$. $\Delta R^{is}/R$ and Ψ affect the birefringent contribution to the RD signal. When performed at some degree of oblique incidence ($\mathbf{r}_p\neq\mathbf{r}_s$), the RDS technique tends to collect isotropic reflectivity contributions. Note that in order to remove the isotropic contribution for an ordered sample, RDS data from random alloy samples are of less use, because the average dielectric function $\in$ changes due to the redshift of the fundamental-gap transition as well. This problem can be circumvented with ellipsometry (determines $\in$ and d) and RDS, as demonstrated in this work.[54]

[1] A. Zunger and S. Mahajan, in *Handbook of Semiconductors*, 2nd ed., edited by S. Mahajan (Elsevier, Amsterdam, 1994), Vol. 3b.

[2] If the random alloy is nonstoichiometric ($x\neq0.5$), η can only vary between $0\leqslant\eta/2\leqslant\min\{x,1-x\}$. Our samples were grown lattice matched to GaAs in which case $x=0.48$. The lattice matching condition is necessary to avoid strain induced birefringence. For derivation of the order parameter η, however, we assume the ideal composition $x=0.5$. The $(Al_{0.48}Ga_{0.52})_{0.5}In_{0.5}P$ is then referred to as $Al_{0.48}Ga_{0.52}InP_2$. One may consider the remaining 0.02 Ga as being located at a Group III site randomly.

[3] A. Zunger, MRS Bull. **22**, 20 (1997).

[4] S.-H. Wei and A. Zunger, Phys. Rev. B **49**, 14 337 (1994).

[5] S.-H. Wei, A. Franceschetti, and A. Zunger, Phys. Rev. B **51**, 13 097 (1995).

[6] S.-H. Wei, D. B. Laks, and A. Zunger, Appl. Phys. Lett. **62**, 1937 (1993).

[7] S.-H. Wei and A. Zunger, Phys. Rev. B **57**, 8983 (1998).

[8] A. Gomyo, T. Suzuki, and S. Iijima, Phys. Rev. Lett. **60**, 2645 (1988).

[9] T. Kanata, M. Nishimoto, H. Nakayama, and T. Nishino, Phys. Rev. B **45**, 6637 (1992).

[10] A. Mascarenhas, S. Kurtz, A. Kibbler, and J. M. Olson, Phys. Rev. Lett. **63**, 2108 (1989).

[11] M. Schubert, B. Rheinländer, and V. Gottschalch, Solid State Commun. **95**, 723 (1995).

[12] P. Ernst, C. Geng, F. Scholz, H. Schweizer, Y. Zhang, and A. Mascarenhas, Appl. Phys. Lett. **67**, 2347 (1995).

[13] G. E. Pikus and G. L. Bir, *Symmetry and Strain Induced Effects in Semiconductors* (Wiley, New York, 1974).

[14] C. W. Higginbotham, M. Cardona, and F. H. Pollak, Phys. Rev. **184**, 821 (1969).

[15] R. Wirth, A. Moritz, C. Geng, F. Scholz, and A. Hangleiter, Phys. Rev. B **55**, 1730 (1997).

[16] S.-H. Wei and A. Zunger, Appl. Phys. Lett. **64**, 757 (1994).

[17] J. S. Luo, J. M. Olson, S. R. Kurtz, D. J. Arent, K. A. Bertness, M. E. Raikh, and E. V. Tsiper, Phys. Rev. B **51**, 7603 (1995).

[18] J. S. Luo, J. M. Olson, Y. Zhang, and A. Mascarenhas, Phys. Rev. B **55**, 16 385 (1997).

[19] M. Schubert, B. Rheinländer, E. Franke, I. Pietzonka, J. Škriniarová, and V. Gottschalch, Phys. Rev. B **54**, 17 616 (1996).

[20] R. Wirth, H. Seitz, M. Geiger, J. Porsche, F. Scholz, and A. Hangleiter, J. Appl. Phys. **83**, 6196 (1998).

[21] R. Wirth, J. Porsche, F. Scholz, and A. Hangleiter, Phys. Rev. B **60**, 1582 (1999).

[22] A. Mascarenhas, B. Fluegel, Y. Zhang, J. F. Greisz, and J. M. Olson, Phys. Status Solidi A **64**, 477 (1997).

[23] P. Kiesel, T. Kippenberg, E. Greger, M. Moser, U. Hilburger, J. Krauss, G. Schmiedel, and G. H. Döhler, Physica E (Amsterdam) **2**, 599 (1998).

[24] P. Y. Yu and M. Cardona, *Fundamentals of Semiconductors* (Springer, Berlin, 1995).

[25] F. Alsina, M. Garriga, M. I. Alonso, J. Pascual, C. Geng, P. Ernst, and F. Scholz, Cryst. Res. Technol. **31**, 205 (1996).

[26] Despite the fact that the sample grown on (001)-GaAs should obey double-variant ordering, its optical properties observed here are uniaxial with an optical axis coincident with the $[1\bar{1}1]$ direction.

[27] S. Adachi, Phys. Rev. B **35**, 7454 (1987).

[28] S. Adachi, *Physical Properties of III-V Semiconductor Compounds* (Wiley-Interscience, New York, 1992).

[29] M. Kondow, H. Kakibayashi, and S. Minagawa, Phys. Rev. B **40**, 1159 (1989).

[30] R. M. A. Azzam and N. M. Bashara, *Ellipsometry and Polarized Light* (North-Holland, Amsterdam, 1977).

[31] M. Schubert, Thin Solid Films **313/314**, 324 (1998).

[32] M. Schubert, B. Rheinländer, B. Johs, C. M. Herzinger, and J. A. Woollam, J. Opt. Soc. Am. A **13**, 875 (1996); **13**, 1930 (1996).

[33] M. Schubert, Phys. Rev. B **53**, 4265 (1996).

[34] J.-D. Hecht, A. Eifler, V. Riede, M. Schubert, G. Krauß, and V. Krämer, Phys. Rev. B **57**, 7037 (1998).

[35] M. Schubert, T. E. Tiwald, and J. A. Woollam, Appl. Opt. **38**, 177 (1999).

[36] B. O. Seraphin and N. Bottka, Phys. Rev. **145**, 628 (1966).
[37] D. E. Aspnes, in *Handbook on Semiconductors*, edited by M. Balkanski (North-Holland, Amsterdam, 1980), Vol. 2, pp. 109–179.
[38] M. Cardona, F. H. Pollak, and K. L. Shaklee, J. Phys. Soc. Jpn. (Suppl.) **21**, 453 (1993).
[39] D. E. Aspnes and A. A. Studna, Phys. Rev. Lett. **54**, 1956 (1985).
[40] D. E. Aspnes, J. Vac. Sci. Technol. B **3**, 1498 (1985).
[41] D. E. Aspnes and A. A. Studna, Phys. Rev. B **27**, 985 (1983).
[42] J. F. Elman, J. Greener, C. M. Herzinger, and B. Johs, Thin Solid Films **313/314**, 814 (1998).
[43] W. H. Press, B. P. Flannery, S. A. Teukolsky, and W. T. Vetterling, *Numerical Recipies in C* (Cambridge University Press, Cambridge, 1988).
[44] M. Schubert, J. A. Woollam, G. Leibiger, B. Rheinländer, I. Pietzonka, T. Saß, and V. Gottschalch, J. Appl. Phys. **86**, 2025 (1999).
[45] C. M. Herzinger, P. G. Snyder, B. Johs, and J. A. Woollam, J. Appl. Phys. **77**, 1715 (1995).
[46] S. Adachi, S. Ozaki, M. Sato, and K. Ohtsuka, Jpn. J. Appl. Phys. **35**, 537 (1996).
[47] S. Ozaki, S. Adachi, M. Sato, and K. Ohtsuka, J. Appl. Phys. **79**, 439 (1996).
[48] K. Asami, H. Ashai, S. Gouda, Y. Kawamura, and H. Tanaka, Solid State Commun. **70**, 33 (1989).
[49] S. H. Wei and A. Zunger, Phys. Rev. B **51**, 14 110 (1995).
[50] D. W. Berreman, J. Opt. Soc. Am. **62**, 502 (1972).
[51] I. Abdulhalim, L. Benguigui, and R. Weil, J. Phys. (France) **46**, 815 (1985).
[52] H. Wöhler, M. Fritsch, G. Haas, and D. A. Mlynski, J. Opt. Soc. Am. A **5**, 1554 (1988).
[53] P. Yeh, *Optical Waves in Layered Media* (John Wiley & Sons, New York, 1988).
[54] G. B. Stringfellow, MRS Bull. **22**, 27 (1997).